Journal of Nuclear Materials 635 (2027) 157169

Contents lists available at ScienceDirect

Journal of Nuclear Materials

journal homepage: www.elsevier.com/locate/jnucmat

Qualification of EUROFER97 and design rule validation for ITER TBM: EUROfusion contribution

D. Terentyev [a,*], P. Lamagnère [b], Y. Lejeail [b], G. Perez [c], M. Walter [d], T.T.M. Nguyen [d], M. Carrington [e], C. Caes [c], E. Leon Gutierrez [f], M. Serrano [f], N. García-Rodríguez [f], R. Hernandez [f], J. Hure [c], J.B. Pontier [c], E. Gaganidze [d], J. Aktaa [d], E. Perelli Cippo [g], Dario Ripamonti [g], V. Lezaud-Chaillioux [c], A. Zinovev [a], I. Szenthe [h], D. Bernardi [i], G. Pintsuk [j], G. Aiello [k], Yann Carin [l], Zmitko Milan [l], Salvatore D'Amico [l], Poitevin Yves [l]

[a] Belgian Nuclear Research Centre, SCK CEN, Mol, 2400, Belgium
[b] CEA-Cadarache, 13108 Saint Paul-Lez-Durance, France
[c] CEA-SACLAY, 91191 GIF SUR YVETTE CEDEX, France
[d] Karlsruhe Institut für Technologie, Hermann-von-Helmholtz-Platz 1, 76344 Eggenstein-Leopoldshafen, Germany
[e] United Kingdom Atomic Energy Authority, Culham Centre for Fusion Energy, Culham Science Centre, Abingdon, Oxon OX14 3DB, UK
[f] CIEMAT. Avd. Complutense 40, 28040 Madrid, Spain
[g] ISTP, Consiglio Nazionale delle Ricerche, Via Roberto Cozzi 53, 20125 Milano, Italy
[h] HUN-REN CER, KFKI Campus, 1121, Budapest, Konkoly-Thege Miklós út 29-33, Hungary
[i] ENEA C.R. Brasimone, 40032 Camugnano (BO), Italy
[j] Forschungszentrum Jülich GmbH, Institute of Fusion Energy and Nuclear Waste Management – Plasma Physics, 52425 Jülich, Germany
[k] EUROfusion PMU, Boltzmannstraße 2, 85749, Garching, Germany
[l] Fusion For Energy, Josep Pla, 2, Torres Diagonal Litoral B3, Office 07/19, 08019 Barcelona, Spain

HIGHLIGHTS

- Overview of qualification program for EUROFER97 is presented.
- New neutron irradiation results are presented.
- Main lessons learned are presented.
- Remaining gaps for high priority test program are summarized.

ARTICLE INFO

Keywords:
EUROFER97
ITER
Test blanket module
RCC-MRx

ABSTRACT

In future fusion power plants (DEMO, CFETR or SPARC) the Breeding Blanket is the component in which tritium, one of the fuel elements for the fusion reaction, is generated. Various Test Blanket Module (TBM) concepts are planned for installation in ITER, where each TBM is considered as nuclear pressurized equipment according to French regulation. The structural material for the European TBM is EUROFER97, a Reduced Activation Ferritic Martensitic (RAFM) steel. Fusion for Energy (F4E) and the EUROfusion Consortium are collaboratively engaged to codify EUROFER97 to complete implementation in RCC-MRx.

List of abbreviations: RAFM, Reduced activation ferritic steel; RCC-MRx, Design and construction rules for mechanical components of advanced reactors, Research reactors and fusion reactors; F4E, Fusion for energy; PPR, Probationary phase rules; LCF, Low cycle fatigue; FCG, Fatigue crack growth; RPS, Reference procurement specification; TIG, Tungsten inert gas welding; HIP, Hot isostatic pressing welding; UC, Unloading compliance; PD, Potential drop; C-F, Creep-fatigue; RT, Room temperature; MTR, Material test reactor; UTS, Ultimate tensile strength; YS, Yield stress; DBTT, Ductile to brittle transition temperature; IPFL, Immediate plastic flow localization; WCLL, Water cooled lead lithium; HCPB, Helium cooled pebble bed; HCCP, Helium cooled ceramic pebble; TBS, Tritium breeding system; CT, Compact tension sample; DCT, Disk compact tension sample; NDR, Normalization data reduction; L-M, Larrson-Miller diagram; MPH, Material property handbook; TEM, Transmission electron microscopy; CMOD, Crack mouth opening displacement; FEM, Finite element method; DONES, DEMO oriented neutron source; SSTT, Small specimen test techniques; ORNL, Oakridge national lab; HFIR, High flux isotope reactor; HFR, High flux reactor.

* Corresponding author at: SCK-CEN, Boeretang, 200, 2400 Mol, Belgium.
E-mail address: dterenty@sckcen.be (D. Terentyev).

https://doi.org/10.1016/j.jnucmat.2026.157169
Received 22 January 2026; Received in revised form 11 August 2026; Accepted 19 October 2026
Available online 20 October 2026
0022-3115/© 2026 The Authors. Published by Elsevier B.V. This is an open access article under the CC BY-NC-ND license (http://creativecommons.org/licenses/by-nc-nd/4.0/).

This paper reviews the scope of the mechanical tests required to complete the codification of EUROFER97, which include (i) mechanical properties according to existing standards; (ii) bespoke tests to validate the design rules; (iii) assessment of neutron induced aging and (iv) bespoke tests to develop the constitutive material's models. In the review of the program, attention is given to the properties of EUROFER97 Batch 3 and Batch 4, used for the production of TBM mock-ups, in relation to existing data for previous batches. Results from collaborative test campaigns are given for fatigue, creep and fracture mechanics properties as well as from the first neutron irradiation campaigns extending our knowledge to high-temperature range (450–550 °C). Progress in design rules validation (ratcheting, plastic flow instability in non-irradiated and irradiated condition and creep fatigue) is highlighted. Finally, a number of challenges faced during the five year implementation campaign, preliminary lessons learned and further planning for the completion of high priority tests are presented.

1. Introduction

In a tokamak-based fusion power plant such as DEMO, the Breeding Blanket is an In-Vessel system facing the plasma that has to supply tritium in excess to the amount used as fuel to self-sustain the fusion reaction [1]. It is foreseen that a set of different Test Blanket Module (TBM) concepts will be installed on ITER to validate its design and functioning in nuclear fusion environment. Importantly, each TBM is considered as pressurized equipment (some of which even nuclear pressurized equipment) according to French regulation and therefore requires stringent regulatory material requirements, design and structural integrity assessment[1] to ensure safety during operation and maintenance [2]. In the case of ITER, RCC-MRx is the code selected for the design and construction, and therefore the structural integrity of the TBMs must be validated in accordance with its design rules [3]. The implementation of this assessment implies the knowledge of the operational loads and environmental conditions (thermal, mechanical, neutron, gamma), the failure modes for which the rules must be validated and the material properties to be used in this assessment. The harvesting and codification of the material properties for the structural material of the European TBM [4], being EUROFER97 reduced activation ferritic martensitic (RAFM) steel [5], is the joint endeavor of Fusion for Energy (F4E) and the EUROfusion Consortium [6].

Based on conventional 8–12%CrMoVNb steels, RAFM steels have been developed for fusion application by substitution of Mo and Nb with W and Ta and reduction of impurities (e.g. Cu, Al) in order to accelerate the decay of post-irradiation dose and reduce the time to store the materials as low-level wastes after reactor shut-down [7]. In EU, the 9% CrWTa RAFM steel named EUROFER97 has been developed and four industrial batches and various semi-finished products have been produced by Boehler, Austria (Batch 1) and Saarschmiede, Germany (Batches 2, 3, 4) [8]. EUROFER97 has been chosen as structural material for the ITER TBM, whose design and manufacturing will be covered by the nuclear code RCC-MRx [3]. In the latest edition of the RCC-MRx code, physical and mechanical properties of EUROFER97 products used for the design have been implemented in Probationary Phase Rules. Additional experimental results and analysis are expected for full qualification and validation of allowable curves for EUROFER97.

The scope of the EUROfusion program includes a dedicated Work Package "Materials" [9], where amongst others the qualification of EUROFER97 and its welded joints is one of the high-level objectives during 2021–2027. The objective of the qualification program is to resolve the remaining issues and validate the design criteria for the use of EUROFER97 as a structural material for the ITER TBM. The consolidated results will contribute to build and update the material data file [10] required to use materials and products covered by the RCC-MRx code.

The core contribution of the present paper consists of the review of the list of mechanical tests required for the codification of EUROFER97 in the RCC-MRx along currently existing gaps to be filled, most recent experimental results of various mechanical tests done on Batch 3 and Batch 4 EUROFER97, first neutron irradiation data for tensile, creep and fracture toughness obtained on Batch 3 and Batch 4, examples of bespoke mechanical tests required for the validation of the RCC-MRx design rules.

The present paper is organized as follows: Section 2 provides the approach for the remaining actions required for the codification, Section 3 provides examples of most recent results of various mechanical test campaigns, Section 4 delivers the discussion and Section 5 concludes the paper.

2. Approach for the codification of EUROFER97

Although EUROFER97 is already introduced in the RCC-MRx under the Probationary Phase Rules, a number of gaps should be closed to support the TBM conformity assessment. Therefore, the ongoing qualification program implies the actions needed to complete the codification of EUROFER97 under RCC-MRx, and these actions are prioritized as: (i) start-up TBM characterization; (ii) full TBM characterization and (iii) beyond ITER TBM characterization [5]. The scope of the tests for each priority is provided in Table 1.

The task breakdown structure and specific types of tests are provided in Table 2. Several types of tasks/tests are required, namely: (i) mechanical testing according to existing standards to populate the RCC-MRx Material Data file; (ii) non-standard tests to validate the design rules; (iii) long-term creep tests to determine the negligible creep domain and define allowables; (iv) neutron irradiation and post irradiation examination to assess neutron induced aging effects. Although already being quite massive, these tasks represent high priority actions required to complete the start-up TBM characterization and populate the gaps in RCC-MRx enabling its next update in 2028.

In what follows, we provide a review of the ongoing qualification program focusing on high priority studies to fulfill the needs of ITER TBMs. Particular attention is given to the confirmation of the properties of EUROFER97 Batch 3 and Batch 4, used for the production of small-scale TBM mock-ups (sub-components). Fig. 1 provides an overview of the evolution of the industrial production of EUROFER97 steel which counts four batches up to now. Batch 1 and 2 were used in the past [11, 12] to establish the first version of EUROFER97 Material Properties Handbook [13] as well as to provide the first assessment of the irradiation effects [14,15]. In the present work, we investigate properties of Batch 3 and 4, for which the open access information is essentially limited today. Batch 3 has been issued for the development of the Material File for RCC-MRx for base metal, while Batch 4 was used to fabricate TBM component mock-ups and perform welding studies. In this work we provide examples of the joined test campaigns carried out by several labs for the assessment of fatigue, creep and fracture mechanics properties. Furthermore, the results of the first neutron irradiation campaigns performed to extend our knowledge to the high

[1] Beside the structural integrity assessment covered by the RCC-MRx code, there are also the essential safety requirements (in particular PED Annex I par. 4) that are required by the PED and ESPN. Hence, considerable amount of results obtained in this programme are actually used in the NPMA (regulator compliance on material requirements), some of which are not codified through RCC-MRx.

temperature limit (450–550 °C) are provided and the progress on the validation of the design rules (specifically for plastic flow instability, ratcheting and creep-fatigue) is highlighted. Finally, challenges faced during the first five years of program implementation, preliminary lessons learned and the current time planning for the completion of high priority tests is presented.

The qualification program planned within 2021–2027 covers high priority tasks to be fulfilled before end 2025 and some medium priority tasks involving long duration tests up to 2027. The main topics of investigation during this first phase are:

- Evaluation of ratchetting behavior and development of an efficiency diagram for application of the RCC-MRx ratcheting design rule;
- Demonstration of the applicability of the new provisional design rule dealing with creep-fatigue damage of steels susceptible to cyclic softening. This rule has been implemented in the latest edition of RCC-MRx on the basis of the original procedure given in [16];
- Determination of negligible creep curve and additional time to rupture and creep strain rate;
- Effect of neutron irradiation on tensile properties, on ductile fracture toughness, on irradiation creep, and on the plastic flow localization phenomenon;
- Characterization of the mechanical properties of welded joints before and after irradiation;
- Extension of the material database [13] by adding results from various EUROFER97 batches and products as requested by the RCC-MRx in order to complete the Material File. Additional results are expected from room to high temperature (600 °C) for Low Cycle Fatigue (LCF), Fracture Toughness (J_{1c} and J-R curves) and Fatigue Crack Growth (FCG) rate.

The following specific actions for EUROfusion and F4E are identified to complete the integration of EUROFER97 in the RCC-MRx code:

- Complete the Material File with the following feedback:
  - Feedback on industrial experience for procurement and manufacturing
  - Feedback on weldability and industrial experience for welding procedure qualification
- Provide justification for the applicability of the RCC-MRx Design Rules (new design rules if necessary)
- Consolidate and Complete Reference Procurement Specification (RPS, RCC-MRx Tome 2):
  - Consolidate RPS for plates
  - Introduce RPS for bars and tubes products of EUROFER97
- Complete the Properties Group (A3.19AS for base metal, A9.19AS for welds):
  - Consolidate physical properties (Thermal expansion, Young's modulus, Magnetic properties)
  - Update negligible creep domain and irradiation boundaries
  - Update basic mechanical database using new batches (application of AFCEN Technical Publication)
  - Add Fracture Mechanics properties (J_{1C}, J-r, da/dn) before and after neutron irradiation
  - Determine welding coefficients for TIG and HIP joints (J_m, J_t, J_r, J_f)
  - Provide Specific Design Rules for EUROFER97: Efficiency Diagram, Creep-Fatigue, update S_{em} and S_{et} allowable stresses.

3. Results

3.1. Operational conditions and loads for EUROFER97 in European TBM designs

ITER envisages two TBM designs to be installed: water-cooled lead-lithium (WCLL) and helium-cooled pebble bed (HCPB) concepts.[2] Table 3 summarizes the main features of these two designs, whereas for the present work the operational temperature range is most important. As one can see from the table, in the design-defined range, the operational temperature of EUROFER97 falls in the range of 295 – 550 °C. However, in the event of pressure drop, the temperature could exceed 550 °C, which is why the assessment of creep strength and creep-fatigue endurance above 550 °C is essential.

In addition to the heat exposure during the plasma discharge, the TBM will be exposed to neutron irradiation through the whole thickness of the component. In particular, in the First Wall components directly exposed to the plasma, fast neutrons will also generate He and H atoms due to the interaction with Fe atoms and subsequent transmutation reaction with the rate of ~10 He appm/dpa and ~40 H appm/dpa. An example of the dpa distribution through the wall thickness of blanket is provided in Fig. 2(a), an example is given for DEMO. The distribution of the temperature on different parts of EUROFER97 components is given in Fig. 2(b), which shows that the backside of the TBM operates at about 300 °C while the front side and near breeding zone structures operate at about 550 °C. Given that the plasma discharge operation imposes instabilities (so called edge localized modes) and disruption events (transients) as well as vertical displacement events [17], a number of mechanical, thermal and combined loads will exert on the structural components of the TBM. As a result, a number of specific mechanical properties should be obtained for the characterization of the reversible and irreversible deformation of the structural components, namely: uniaxial tensile, ductile fracture toughness, uniaxial ratcheting, uniaxial low cyclic fatigue, tension-torsion cyclic fatigue, creep, creep-fatigue and a number of bespoke mechanical tests required for the derivation of the material's constitutive behavior.

Table 1
Scope of TBM tests subdivided in three implementation phases.

	Start-up TBM characterization	Full TBM characterization	Beyond TBM characterization
Scope of tests	Mechanical properties for preliminary design of the two EU TBMs, at least with respect to the normal operation in the later ITER phases. To limit testing times, the test parameters (type of products, temperatures, holding times, irradiation levels, etc.) are reduced in order to cover at least the boundaries of TBM operating conditions.	These tests are required to fulfill minimum needs for EUROFER97 qualification for the final TBM design and assess the operational domain of TBM outside normal operation.	These tests are required to achieve the full qualification of EUROFER97 in RCC-MRx beyond the TBM operational domain, providing material data applicable to DEMO-relevant conditions.
Estimated time at completion	2023	2025–2027	2029

[2] Please note that the former HCPB TBM concept has been renamed the Helium-Cooled Ceramic Pebble (HCCP) TBM following the establishment of the EU-Korea partnership agreement. The main features of the HCPB TBS have been retained, and the analyses and calculations previously performed for the HCPB therefore remain applicable to the HCCP TBS.

The basic static mechanical properties such as tensile and fracture toughness are sufficient only to address monotonic mechanical loads. When it comes to combined loads, e.g. cyclic thermo-mechanical fatigue, one needs to deliver both cyclic fatigue endurance and time-dependent creep rate. The structural integrity assessment is furthermore complicated due to the presence of neutron irradiation, which (i) serves as source of diffusing point defects and hydrogen transmutation; (ii) produces nanometric lattice defects built up as a result of continuous operation and (iii) causes formation of He bubbles, given that He is practically insoluble in steels. In the case of ITER TBM, the maximum envisaged irradiation damage at the end of D-T 2 phase should not exceed 3 dpa, and former irradiation studies point to the fact that presence of He at such dpa-level does not provide additional deterioration of the mechanical properties [19]. However, the enhanced diffusion and formation of nanometric voids and dislocation loops does alter creep deformation rate and induces hardening. The latter is expressed as yield stress (Rp0.2) and ultimate tensile stress (Rm) increase, occurring physically due to the obstruction of dislocation movement by irradiation defects. The hardening is especially pronounced in the low operational temperature range (i.e. < 325 °C) and it emerges linearly up to few dpa and then comes to a saturation following a square root dependence. The currently available data set for EUROFER97 on the Rm at $T_{irr} < 340$ °C is summarized in Fig. 3(a). The negative consequence of the hardening is the reduction of the total and uniform elongation, as is shown on Fig. 3(b) and (c), respectively. The latter imposes a risk of ductility exhaustion and immediate plastic flow instability (i.e. immediate necking deformation at the yield point). Finally, with the accumulation of the dpa damage, the ductile-to-brittle (DBTT) transition temperature raises such that it reaches RT around 2–3 dpa, and then saturates at around 150 °C at 50–70 dpa, as shown in Fig. 3(d). One needs to warn that the data presented in Fig. 3 is obtained using fission material test reactors. According to the information obtained using spallation neutron sources (with 20–40 appm He/dpa), the detrimental effect of He transmutation emerges above 10 dpa and this pushes the actual DBTT to higher values due to so-called He embrittlement. Nevertheless, in the case of ITER-relevant neutron fluence, He effects can be ignored.

The information presented on Fig. 3 provides the basis for the selection of several dpa levels at which the mechanical properties should be obtained and then interpolated to provide the trend curves for the design. In this specific case, the following properties have been considered: Rm – ultimate tensile stress (aka UTS), εt – total elongation, εu – uniform elongation, DBTT – ductile to brittle transition temperature taken from impact tests. The selection of the dpa milestones has been done in the following manner: (i) the change of each property has been normalized over the saturated value, so that each property changes from 0 (non-irradiated state) to unity (saturated value), which is shown in Fig. 4(a). Then, the mean curve is built by averaging the Rp0.2 (yield stress), Rm, εt, εu and DBTT, which is indicated by the thick red curve in Fig. 4(a). This mean curve can be seen as effective mechanical property change and its derivative over dpa would indicate the rate of the property change. The derivative is shown on Fig. 4(b) and therein one can see a characteristic cusp around 0.2–0.4 dpa signifying the dpa level at which the uniform elongation reaches zero. The rate of the property change is becoming very small above few dpa, which is due to the fact that irradiation defect density is established and further irradiation leads to the slow growth of voids and dislocation loops. For the assessment of the irradiation effects for ITER TBM in the case of Batch 3 and Batch 4 EUROFER97, three damage levels were selected: 0.5–0.7 dpa; 1–1.5dpa and 2–2.5 dpa.

Accounting for the various needs of mechanical property delivery,

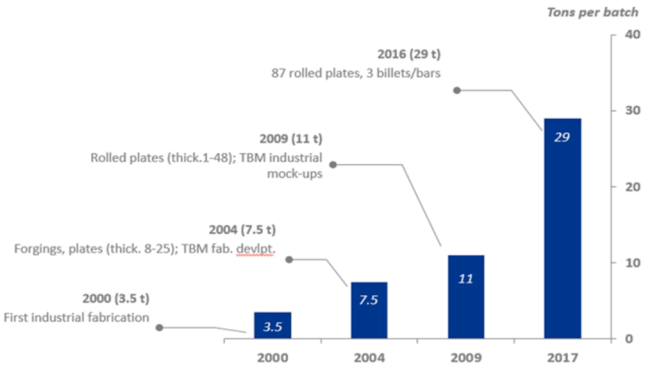


Fig. 1. Evolution of EUROFER97 production.

Table 3
Characteristics of ITER TBMs employing EUROFER97 as structural material. TBS refers to Tritium Breeding System.

	WCLL	HCPB/HCCP
Breeder	PbLi liquid metal (enriched with ^{6}Li)	Li4SiO4 + Li2TiO3 (enriched with 6Li) breeding ceramic pebbles
Coolant	Water in double wall tubes, 295/328 °C (in/out)	He, 300/500 °C (in/out)
Pressure	15.5 MPa	8 MPa (0.4 MPa in breeding zone)
Temperature range	295/550 °C	300–550 °C
PED Level and Category	Cat IV, N2 (TBM-Set)	Cat IV, N2 (TBM-Set)– to

Table 2
Timeline for the specific task implementation executed by EUROfusion consortium.

Non-irradiated Base Metal	Test types	2021	2022	2023	2024	2025	...
Ratcheting	Tension/Torsion Cyclic						
Uniaxial Ratcheting*	Stress-controlled Cyclic Uniaxial						
Creep-Fatigue Interaction	Creep-Fatigue Cyclic Uniaxial						
	Fatigue-Relaxation Cyclic Uniaxial						
Immediate Plastic Flow Localization*	Plain/Notched Tensile						
	Plain/Notched 4 Points Bending						
Fatigue*	Strain-controlled Cyclic Uniaxial						
Creep*	Tensile creep						
Fracture Toughness	Compact Tension (CT)						
Fatigue Crack Growth	Cyclic CT						
Irradiated Base Metal	**Test types**	**2021**	**2022**	**2023**	**2024**	**2025**	**...**
Immediate Plastic Flow Localization	Plain/Notched Tensile						
	Plain/Notched 4 Points Bending						
Tensile Properties*	Cylindrical Tensile						
Irradiation Creep*	Creep pipes						
Fracture Toughness*	CT and DCT						

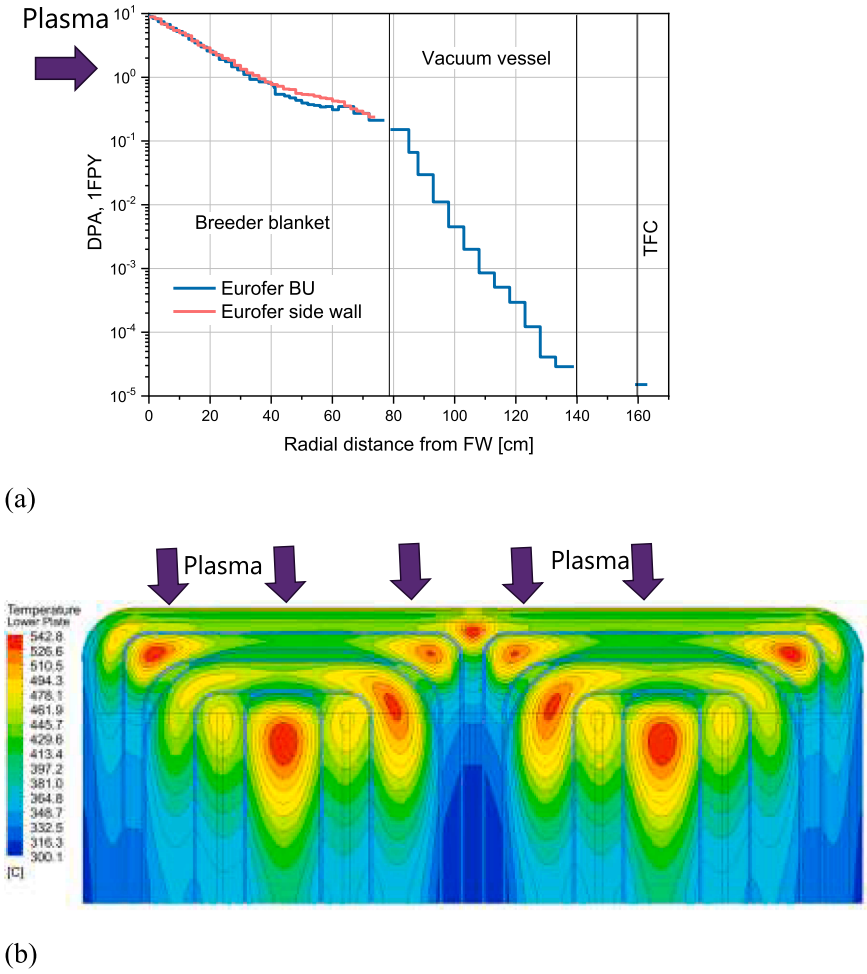


Fig. 2. Illustration of the gradient of dpa and Helium production through the thickness (a) and temperature gradient (b) of the HCPB TBM [18].

the test program has been dispatched across several labs. Seven laboratories collaborating within EUROfusion consortium are involved in the qualification program: UKAEA (UK), CEA (France), CIEMAT (Spain), EK (Hungary), ENEA (Italy), KIT (Germany), SCK CEN (Belgium). Fig. 5 provides an overview of the participating laboratories and associated types of mechanical tests. The neutron irradiation was assigned to BR2 and BRR reactors in Belgium and Hungary, respectively. Germany and France do take part in the post-irradiation examination (together with Belgium and Hungary), which will require exploitation of hot cells and availability of the accredited equipment in there. In addition to the neutron irradiation, a number of bespoke tests has been performed to validate the design rules as well as to obtain the data for the derivation of the material constitutive law under complex loads (i.e. tension-torsion ratcheting, digital image correlation, laser profilometry, etc.). Primary information on the neutron irradiation conditions is provided in sections containing the results of the irradiation tests.

3.2. Low cyclic fatigue, cyclic tension-torsion, ratcheting

The strain-controlled low cyclic fatigue (LCF) tests have been conducted on Batch 3 by five labs according to the ASTM E606 standard on specimens with the gage diameter from 5 to 8.8 mm at strain rate between $1{\cdot}10^{-3}$ and $3{\cdot}10^{-3}$ s^{-1} with strain ratio $e_{min}/e_{max} = -1$ and 0. The test matrix covered the test temperature: RT, 300, 350, 450, 550 °C; and strain ranges $\Delta\mathcal{E}$=0.3, 0.6, 0.8, 1.2, 1.5%. A number of test conditions has been assigned to at least two labs to assess the inter-lab data spread. Example of the fatigue endurance curves is given in Fig. 6(a), (b) and (c) for RT, 450 and 550 °C. The results for Batch 3 are compared with the previous results obtained for Batch 1 and the average curves currently integrated in the Material File. Design curves reported in the current edition of the RCC-MRx are also included. As one can see, the new results are close to the former ones. The update of the material data file and revision of the design curves will be done using the newly obtained data. The change of the stress range (i.e. cyclic softening) at the half-life as a function of strain range is presented in Fig. 7(a), which shows that there is overall good agreement between Batch 1 and 3 datapoints. One can see that with increasing test temperature the stress range diminishes as a result of decreasing yield strength. Finally, it is worth to highlight that the results of the inter-lab tests revealed good agreement between the LCF results, including also the fracture surface investigation, more information can be inferred from Ref. [20]. Most of the LCF tests were performed without significant technical issues, however, at the lowest strain rage (0.3%), the signal from the strain gage was at the level of the technical resolution and even minor variations in the test environment (day/night temperature variation in the room) could cause spurious signal readings and issues to evaluate relevant symmetrization factor $K_s = \sigma_{max}/\Delta\sigma$, after cycling (see Fig. 7(b)).

The effect of cyclic softening of EUROFER97 on the ratcheting behavior is investigated by uni-axial cyclic tests at true stress control and tension-torsion cyclic tests at strain control. The former can be used to validate or improve inelastic cyclic models [21] while the latter are dedicated to the development of elastic design rules to prevent progressive deformation [22].

The uniaxial experiment is performed in a similar way as the LCF

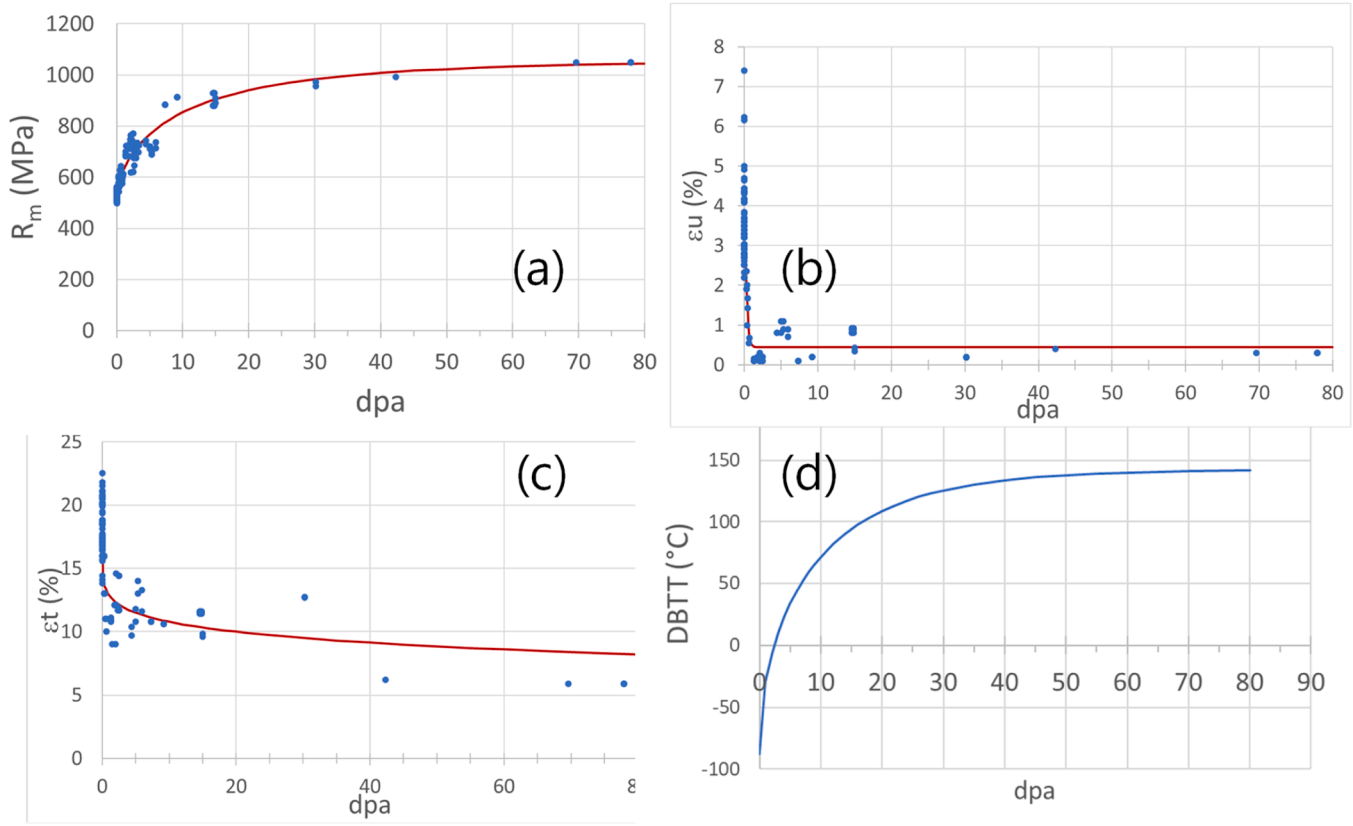


Fig. 3. Evolution of mechanical properties vs. dpa at the irradiation temperature < 340 °C. (a) ultimate tensile strength; (b) uniform elongation; (c) total elongation; (d) ductile-to-brittle transition temperature.

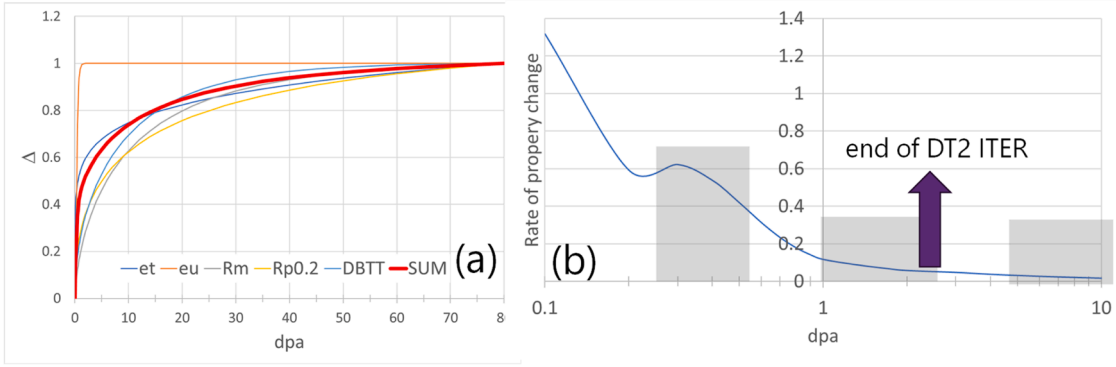


Fig. 4. (a) Normalized measure of degradation of the mechanical property and (b) its derivative over dpa.

tests but instead of having strain-controlled load, the load is true stress controlled using a peak stress ratio $R = s_{min}/s_{max}$ varying from −1.05 to 0. The reference peak stress s_{max} is defined based on the actual yield stress which should be pre-determined for the material subject to the test by standard tensile test at the relevant temperature. The cyclic load is then applied below the yield stress and the test lasts up to the strain when the uniform elongation is reached. The demonstration of the progressive ratcheting deformation is given on Fig. 8(a). The true stress – strain loops are provided for the 1st, 113th and 193rd cycle. One can see that the mean ratcheting strain increases with the number of cycles until the total strain reaches 3.5%, which is close to the uniform elongation at this temperature so that the test is stopped at the onset of necking. The overall objective of these tests is to determine the effect of the peak stress, stress ratio and stress rate on the average ratcheting rate, and thus to provide the datapoints sufficient for the interpolation to be used to validate non-linear constitutive material law under cyclic load. Only Batch 3 was tested. Two labs were engaged in the tests. The average ratcheting rate per cycle $de_{true,\ mean}/dN$ was calculated using the progress of the true mean strain (mean value of both peak tensile- and peak compression strain) from the start up to the end of a test. An example of the results are provided on Fig. 8(b), which shows the effect of test temperature on the average ratcheting rate vs. peak stress. The tests were performed in two labs at R=−0.9, and one can see a good agreement between the labs. Another example is the effect of the R ratio on the ratcheting rate, which is given on Fig. 8(c) for T_{test}=350 °C. One sees that the maximum ratcheting rate occurs around R=−0.95, the ratcheting rate is reducing and then saturates at 10^{-5}/cycle with reducing the R ratio down to −0.5. On the contrary, at R < −1.0, there is a significant increase of the ratcheting rate, which corresponds to the deformation in compression. Here, we should also note that the datapoints obtained two

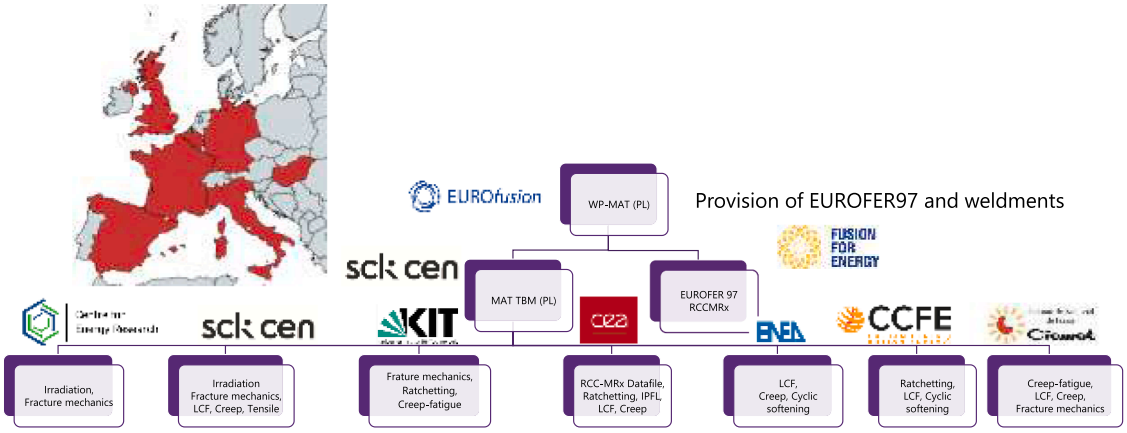


Fig. 5. Dispatch of various tasks among the TBM qualification laboratories participating in the EUROfusion consortium.

labs show good agreement.

Tension - cyclic torsion are the bespoke tests, for which two labs were involved. The objective of such tests is twofold: (i) provide the data to populate the efficiency diagram and (ii) determine the threshold for the ratcheting deformation under primary load. The tests were performed using Batch 3 only. The loading diagram (maintained tensile load and cyclic shear strain vs. time) is schematically shown on Fig. 9(a). The cylindrical tube sample is shown above the figure. The primary load is applied in tension to the heads of the sample, while the secondary cyclic load is applied by torsion to the heads of the sample having the shape of a nut. In such setup, the ratcheting axial elongation and evolution of the torsion stress are measured vs. number of torsion cycles. Fig. 9(b) shows the torsion stress vs. cycle number. One sees that up to 1000 cycles the hardening takes place followed by the softening and eventually failure. At the shear torsion strain amplitude of 0.42% no failure was registered within 350,000 cycles and therefore the test was halted. Axial elongation as a function of fatigue life reflects on Fig. 10(a) the ratcheting behavior. One can see that for the $\Delta\gamma$ =0.42% the ratcheting is negligible, therefore this level of the strain variation can be defined as the threshold at the corresponding tensile load. The ratcheting rate response is strongly dependent on $\Delta\gamma$ in the range 0.5–0.61%. One sees that nearly constant ratcheting rate emerges at $\Delta\gamma$ =0.61%, until the onset of necking ($e_u \approx 1\%$ at 550 °C) is reached. The two points, obtained from the two tests ($\Delta\gamma$ =0.5 and 0.61%), are plotted on the efficiency diagram for P91 and 316 L taken from RCC-MRx, see Fig. 10(b). In addition, the points available from the test campaign on P91 are superimposed on this figure. One can see that the presently obtained points for EUROFER97 lie close to the P91 curve and stay close to the P91 test datapoints, which provides a good confidence in the obtained results. The tests are continued and full test matrix will be completed in 2026.

3.3. *Fracture toughness and fatigue crack growth*

The fracture toughness tests were allocated to three laboratories. The tests were performed on the CT samples with a thickness of 20 mm, designed according to the proportions of ASTM E1820 in T-L orientation. The original intention was to perform tests using unloading compliance (UC) techniques to measure the crack extension during the test (resistance curve procedure). The test matrix covered the following test temperature: RT-300–350–450–550 °C; with at least four tests per test condition with crack extension values, Da= 0.5, 1.0, 1.5 mm and the first test is to be done to reach as large crack extension as possible to steer other tests. In this task, both Batch 3 and 4 are tested.

While performing the first series of tests at room temperature, it was revealed that the application of the UC method is challenging due to the emergence of negative crack-growth signal. The latter emerged at the beginning of the test. This happens likely due to a very steep slope of the J-R basically delivering linear response along the blunting line. To validate the result of the UC method, beside the normalization data reduction (NDR), an additional not initially planned method of potential drop was implemented in one of the testing labs. The J-R curves obtained by the three different methods at RT (for Batch 4) are shown in Fig. 11(a). One can see that the J_Q is considerably lower for the UC method. On the top of those curves, several points are added which correspond to the end-of-test J-Δa values determined post-mortem (basic procedure). One can clearly see that the UC method does not provide a good agreement on J_Q values contrary to the NDR and PD. The origin for the observed discrepancy is believed to be due to the 3D crack extension i.e. the full crack front does not stay in the plane normal to the load axis, which generates a spurious signal to the UC. This issue has been found for both Batch 3 and Batch 4 EUROFER97.

However, at elevated temperature of 300, 350 and 450 °C the UC method was providing reasonable agreement with the NDR. The J-R curves obtained with the UC and post-mortem J-Δa points at 300 °C (for Batch 3) and 350 °C (for Batch 4) are shown in Fig. 11(b) and (c), respectively. A good agreement is clearly seen.

In the second lab, the tests were attempted to be performed with the UC, but due to the above-mentioned issue, the decision was taken to deduct the J-R curves by NDR and basic multi-specimen procedure. Fig. 12(a) shows the J-R curves obtained using NDR at RT (for Batch 3) and the red solid curve corresponds to the multi-specimen method, clearly there is a good agreement. For the tests at 450 °C (Batch 3), the J-R curve was built using the multi-specimen method (see Fig. 12(b)), showing a significant reduction of the J_Q with temperature. Using exactly the same method, specimen size, pre-cracking and test bench the J-R curves for Batch 3 and 4 were obtained at 450 °C, as presented in Fig. 12(c). One can see that Batch 4 exhibits lower toughness, which is consistent with the fact that Batch 4 has lower uniform elongation and has higher yield stress and UTS as compared to Batch 3 [23,24]. Finally, at the upper requested temperature, the J-R curve was constructed using monotonic load (without load-unload compliance by the NDR, see the result on Fig. 12(d). The reason to avoid load-unload cycles originates from the creep-relaxation which was observed to occur above 450 °C during UC measurements.

The effect of temperature is as expected – a reduction of the J_Q with raising the test temperature. Hence, for Batch 3 and CT 20 mm thick sample, J_Q goes down from 750 kJ/m^2 to 640 kJ/m^2. Remarkably, an average J_Q value of ~580 kJ/m^2 determined by the third lab on Batch 3 at 350 °C by using UC, NDRT and Basic methodologies confirms well the trend of the fracture toughness reduction with increasing the test temperature as observed by the first and second labs. The evaluation of the test results by the third lab is still in progress, and the synthesis of all results will be presented in a separate publication.

The fatigue crack growth (FCG) tests were performed using CT

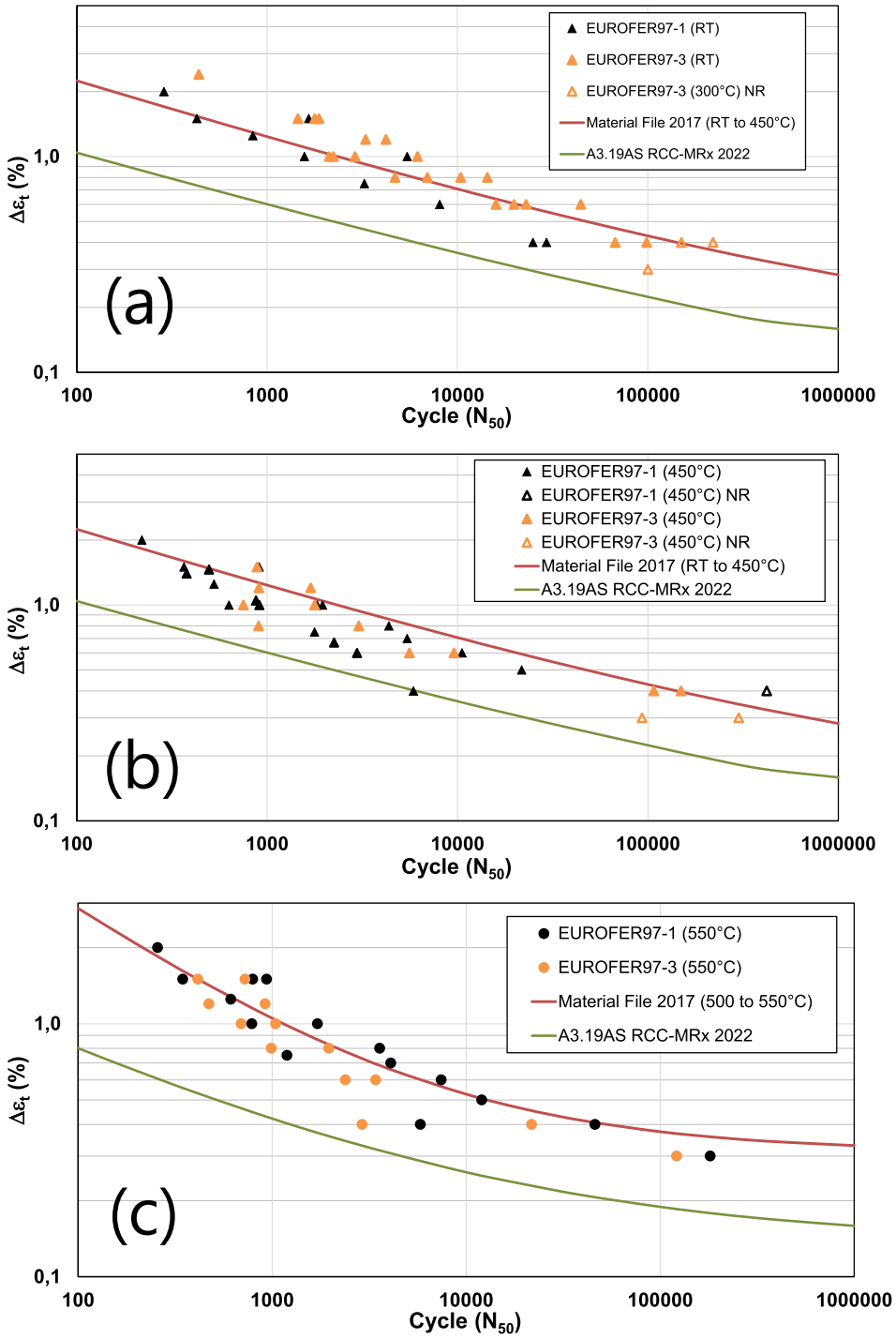


Fig. 6. Fatigue endurance curves. (a) RT tests; (b) 450 °C tests; (c) 550 °C tests.

specimens with W = 20 mm and B = 5 mm in agreement with ASTM E647 standard. The test matrix included T_{test} = 20, 300, 450 °C, stress ratio (R = minStress/maxStress) of 0.1 and 0.5. Test frequence was 5 Hz with a triangular waveform. The tests were performed according to ASTM E647 standard. The test results for RT and 300 °C are plotted in Fig. 13(a) and (b), respectively; for R = 0.1 and R = 0.5. The following observations can be made: (i) the fatigue crack extension increases slightly with raising the test temperature; (ii) the fatigue crack extension increases with raising the R value, which is consistent with reduced crack closure and a lower effective threshold; (iii) both of these trends are consistent with the observations done in T91 steel [25]. Tests are ongoing and the synthesis of the results will be done later.

3.4. Creep

The creep tests were performed in four labs. The tests were done according to ASTM E139–11 standard. Test matrix included the following test temperatures: 400–450–500–550–600–650 °C. Only Batch 3 was tested. The objective of this test campaign was threefold: (i) provide information for the derivation of the negligible creep domain; (ii) tests to reach 1% creep strain and (iii) creep-to-rupture tests. Not all tests are completed yet, and the longest tests will keep on running until

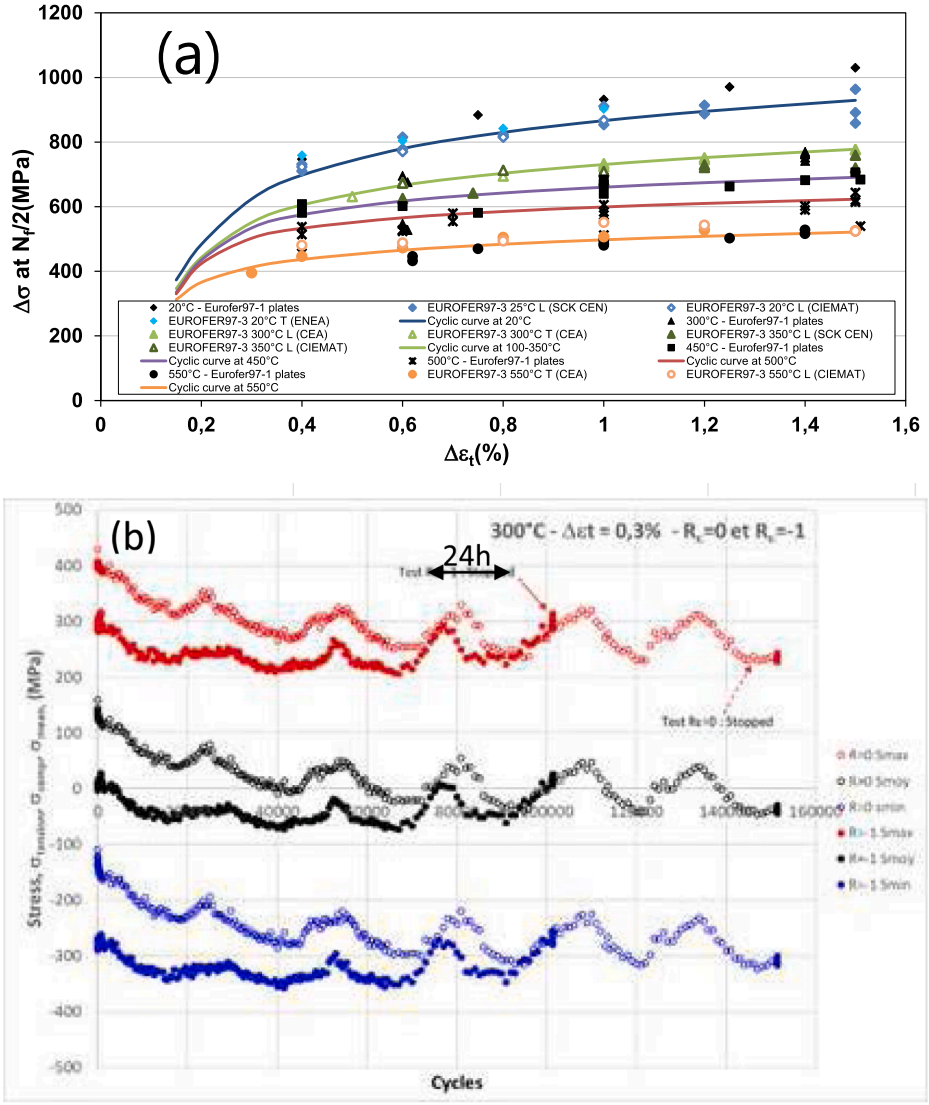


Fig. 7. (a) Softening at the half life and (b) Effect of strain ratio on the cyclic symmetrization at 300 °C.

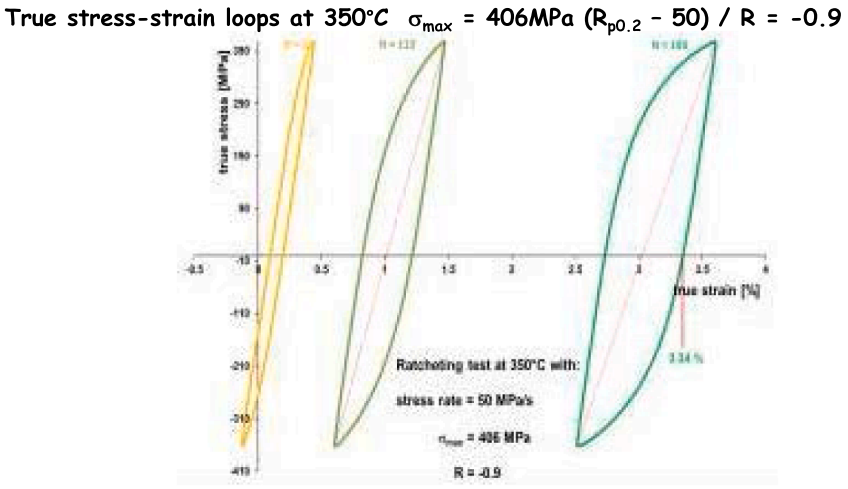
2026 or even 2027. The currently obtained results are summarized on Fig. 14(a), which shows the rupture time vs. creep stress at various test temperatures. The data available for Batch 1 and 2 are also superimposed on the figure. One can see that the trend for the creep life with Batch 3 is very similar to the best fit curves obtained using Batch 1 and 2. However, one can notice that the creep life of Batch 3 is longer at intermediate temperatures (400–450 °C). This has direct implications on the creep-fatigue and fatigue-relaxation tests as will be discussed in the following. The Larsson-Miller (L-M) diagram is constructed on Fig. 14 (b), where all available data points are plotted. One can see that the Batch 3 datapoints fit the L-M curve nearly perfectly, which confirms the consistent creep strength and lifetime of the Batch 3 material.

3.5. Creep-fatigue and fatigue-relaxation

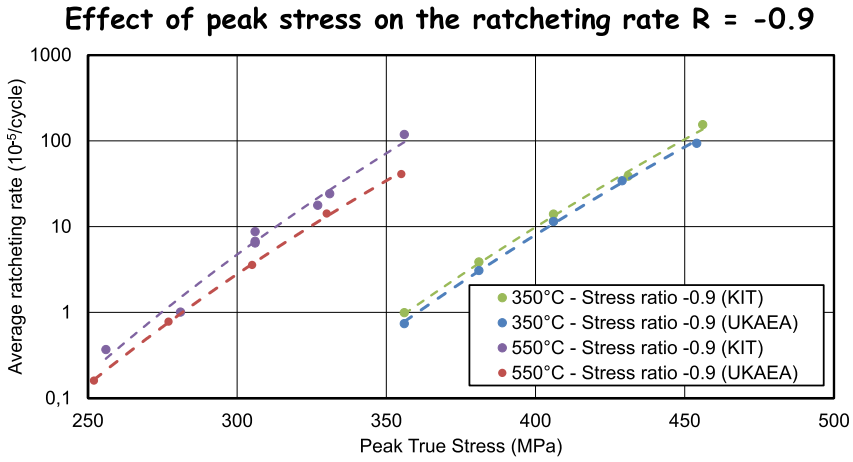
The uniaxial creep-fatigue and fatigue-relaxation tests were performed by two labs using Batch 3 only. The tests were performed using the same sample geometry as for the LCF tests (gage dia. 8.8 mm). The main objective of these tests was the evaluation of the effect of creep damage during dwell in tension and/or compression (at test temperature 450 to 650 °C); and comparison of the lifetime with non-symmetrical LCF tests. Overall, as a result of this test campaign, the dataset covering various Creep and Fatigue usage values was generated to evaluate the design rule for the creep-fatigue interaction and check that no failure occurred in the safe region.

Two types of tests were performed as schematically shown in Fig. 15 (a), namely: (i) creep-fatigue in which a fixed dwell time or fixed creep strain is imposed at the attained stress (load reached under tension or compression at the peak deformation); (ii) fatigue-relaxation in which the peak strain is imposed under tension or compression and stress relaxation is measured given a specific dwell time. An example of the creep-fatigue results is given in Fig. 15(b) which shows the effect of the creep contribution (0.1 −0.5- 1% of creep strain) to the reduction of the life at T_{test}=550 °C and De=1% (dwell in tension). Another example is given for the fatigue-relaxation tests done also at T_{test}=550 °C and De=1%, see Fig. 16(a). The figure shows the pure LCF test result and fatigue-relaxation curve for the strain range of 1% with the dwell time of 200 and 800 s. As one can see, there is no significant effect of the dwell in tension on the fatigue lifetime. On the other hand, by comparing the dwell applied in Tension and in Compression, see test results on Fig. 16 (b) at 450 °C and De=0.6%, the lifetime is much shorter if the dwell is applied in compression.

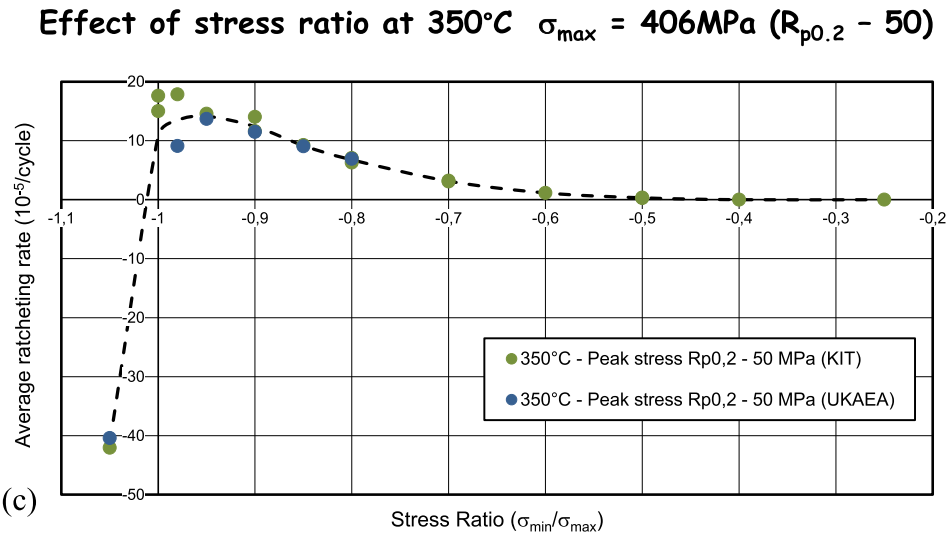
Considering the data of the performed tests, the corresponding creep and fatigue usages were calculated according to the methodology of Aktaa's C-F interaction rule for cyclic softening steels [16], as newly introduced in Probationary Phase rule in the RCC-MRx, and plotted on



(a)



(b)



(c)

Fig. 8. Ratcheting test results. (a) an example of true stress – ratcheting strain loops; (b) effect of peak stress on the average ratcheting rate; (c) effect of R ratio on the average ratcheting rate.

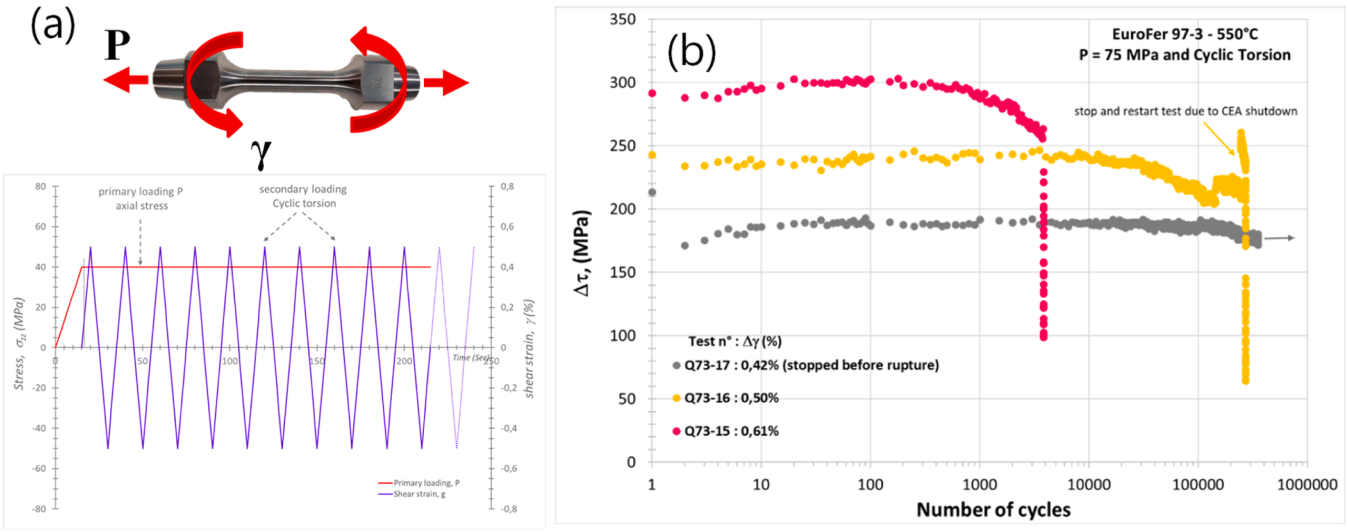


Fig. 9. Tension-torsion results. (a) schematics showing the primary and secondary load diagram and the sample configuration; (b) torsion cyclic stress vs. number of cycles.

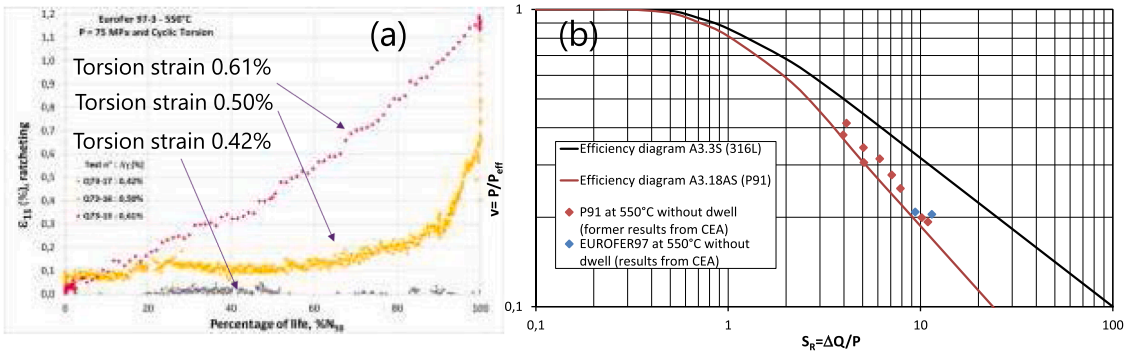


Fig. 10. (a) Axial ratcheting strain as function of torsion cycles and (b) plot of the experimental points on the efficiency diagram for 316 L and P91.

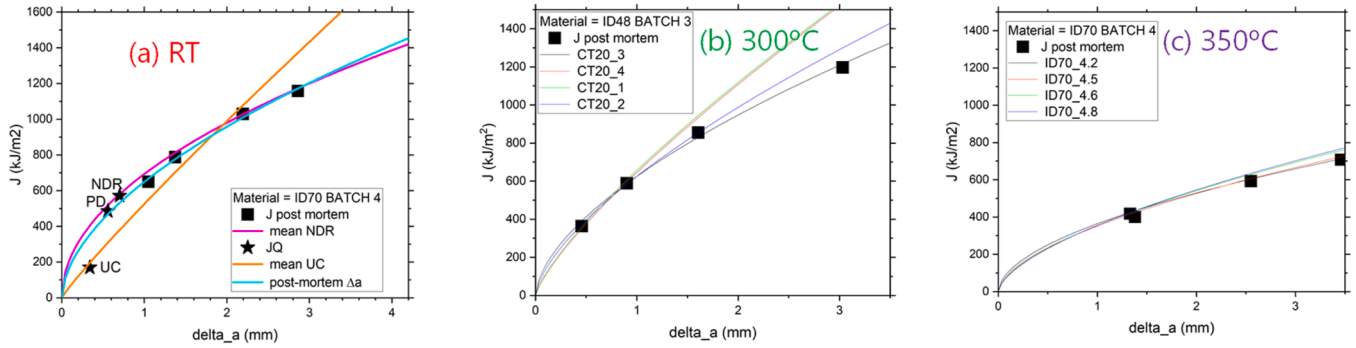


Fig. 11. J-r curves obtained for B3 and B4 using CT20 sample in Lab 1. (a) RT tests for Batch 4 with UC and PD measurement; (b) 300 °C test for Batch 3 with UC measurement; (c) 350 °C test for Batch 4 with UC measurement. T-L sample orientation.

the C-F interaction diagram of the rule (see Fig. 17). The safe and crack initiation domains are indicated on this diagram, where one can see that all obtained points (at rupture) are out of the safe zone delimited by the no crack initiation area in the C-F interaction diagram.

3.6. *Effect of neutron irradiation on tensile properties*

The effect of neutron irradiation on the tensile properties were investigated using miniaturized cylindrical tensile samples with the reduced section length of 10 mm and diameter of 2 mm. The irradiation of tensile samples as well as fracture toughness and bespoke samples for the investigation of the immediate plastic flow location has been performed in BR2 reactor in Belgium. The irradiation was performed inside the fuel element, which represents a hollow cylinder with several highly enriched UAlx concentric plates. The irradiation rig is introduced in the central hole of the fuel element, so that the rig is completely surrounded by the fuel. The samples inside the rig are placed inside the aluminum holder. This maximizes neutron flux and maximum ratio of fast to thermal neutrons. The transmutation rate of the gaseous atoms is ~1.4 appmHe/dpa and ~10–3 appmH^3/dpa. The mean neutron flux on the

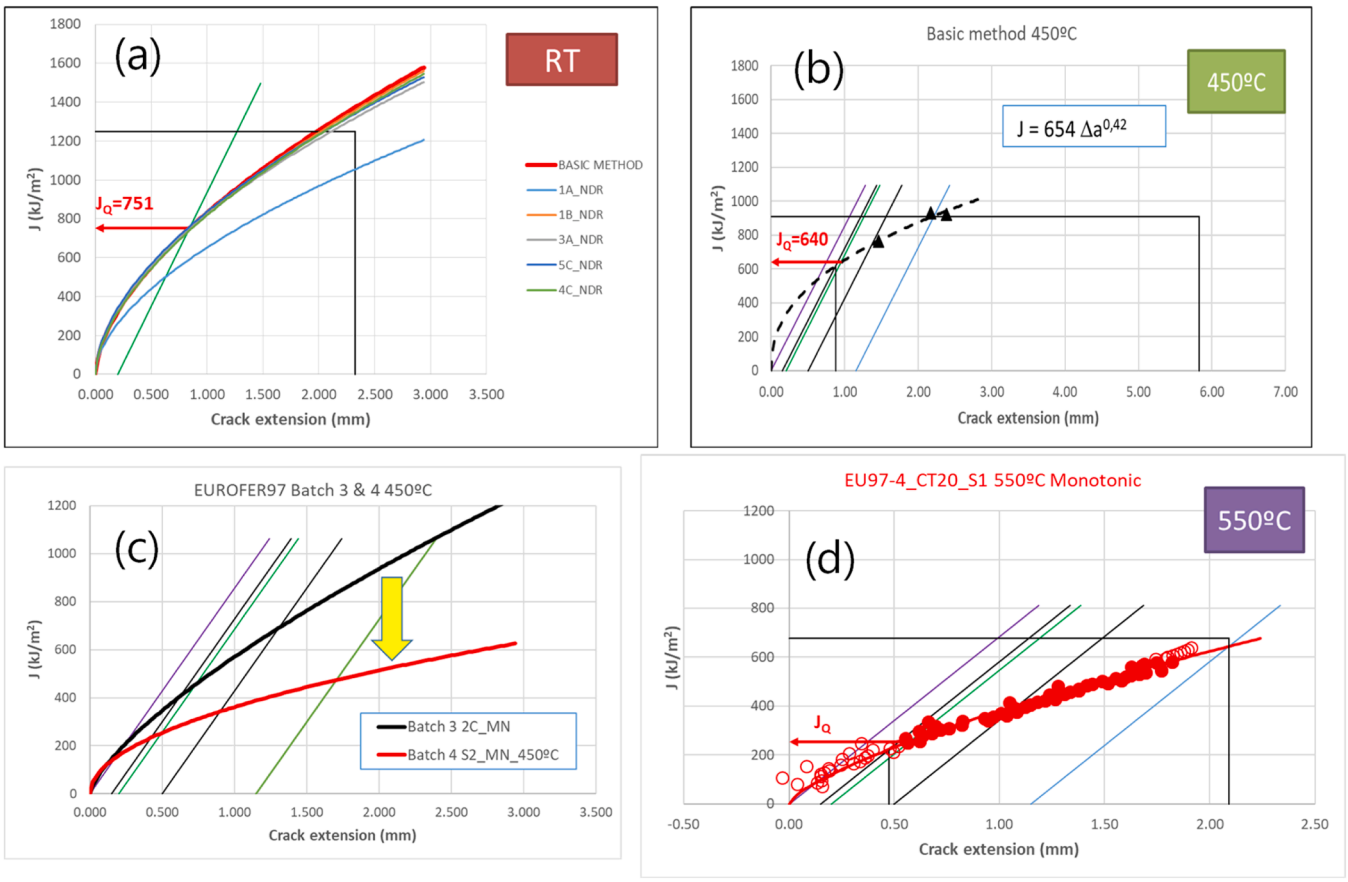


Fig. 12. J-R curves obtained for B3 and B4 using CT20 sample in Lab 2. (a) RT tests for Batch 3; (b) 450 °C test for Batch 3; (c) 450 °C test for Batch 3 and Batch 4; (d) 550C test for Batch 4. T-L sample orientation.

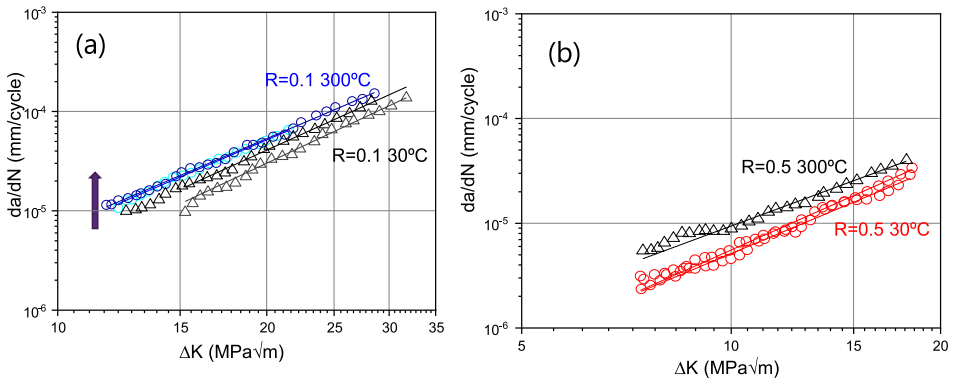


Fig. 13. Fatigue crack growth vs. stress intensity at (a) R = 0.1 and (b) R = 0.5. T-L sample orientation.

Eurofer97 samples is ~6.3E+14 n/cm2, while the neutron flux to which the irradiation device is exposed is ~6.56E+14 n/cm2. The irradiation dose in dpa units was calculated by MCNPX 2.7.0 [26]. The dpa cross sections for Eurofer97 have been prepared from the JENDL4 file (MT444) for the threshold displacement energy of 40 eV. The propagation of the neutron spectrum from the empty irradiation channel through the capsule structure to the samples and transmutation of He and H^3 was calculated based on the ALEPH code developed by SCK CEN and available nuclear databases [27–31]. The neutron spectrum in the BR2 irradiation channel (C79), in the Al holder surrounding the samples and on the samples itself is shown on Fig. 18.

The mechanical tests were performed according to ASTM E8 standard, more information can be found in [24]. Batch 4 samples were irradiated to provide at least three tests per test condition (i.e. a combination of irradiation dose, irradiation temperature and test temperature). The irradiation test matrix included the following irradiation temperatures: 275/300, 350, 450, 550 °C and irradiation doses 0.7 and 1.4 dpa for each irradiation temperature (except one condition T_{irr}=550 °C_1.4 dpa). To ease the presentation of the summary of tensile properties, let us consider an example of the tensile curves before and after the irradiation. The effect of the irradiation (300 °C_1.4dpa) on the engineering stress-strain (SS) curve is shown on Fig. 19. The obtained stress-strain (SS) curves clearly show that the irradiation damage leads to an increase of the yield stress as well as ultimate tensile stress and reduction of the uniform elongation and the total elongation. This is a well-known effect registered in RAFM steels, not exclusively in

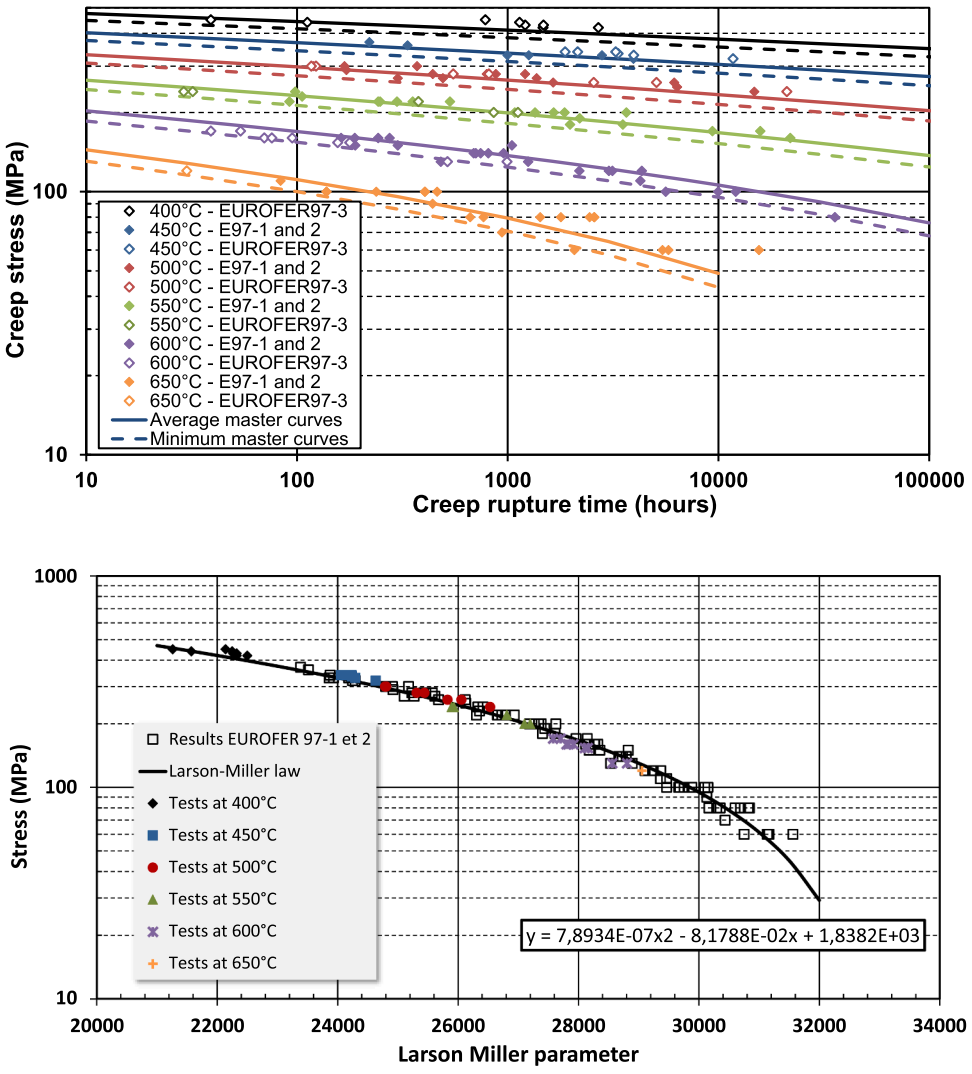


Fig. 14. Creep life and Larsen Miller diagram.

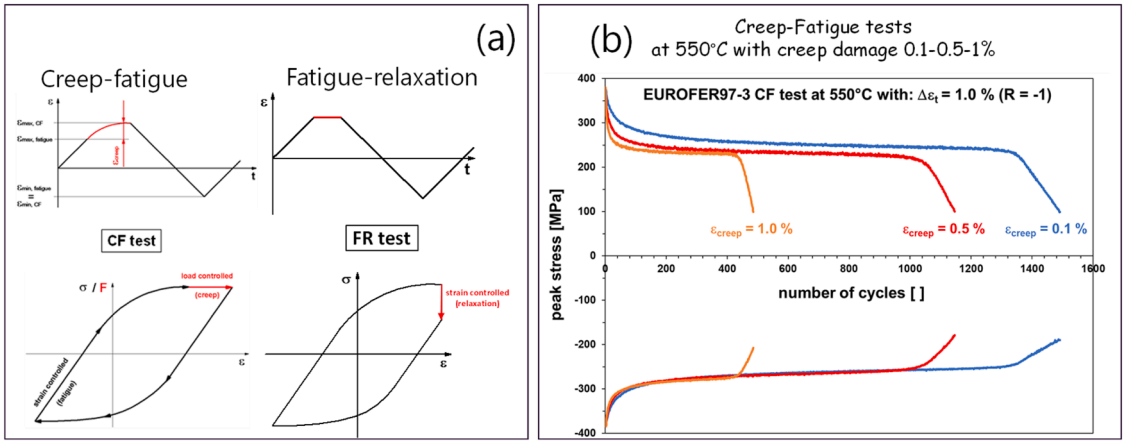


Fig. 15. (a, left) Creep-fatigue test protocol and (b, right) peak stress vs. number of cycles for the creep-fatigue tests performed at 550 °C with dwell in tension. The effect of the applied creep strain on the lifetime for the applied testing conditions is demonstrated.

EUROFER97, which is especially pronounced at irradiation temperature below 350 °C [14]. Although the rupture of the material occurs in a fully ductile manner, the reduction of the uniform elongation to zero triggers the importance of the ductility exhaustion and plastic flow instability prevention rules.

The summary of the tensile properties (YS, UTS, uniform and total elongation) are presented in Fig. 20. The measured values are shown here with spread out circles, which is compared with the corresponding

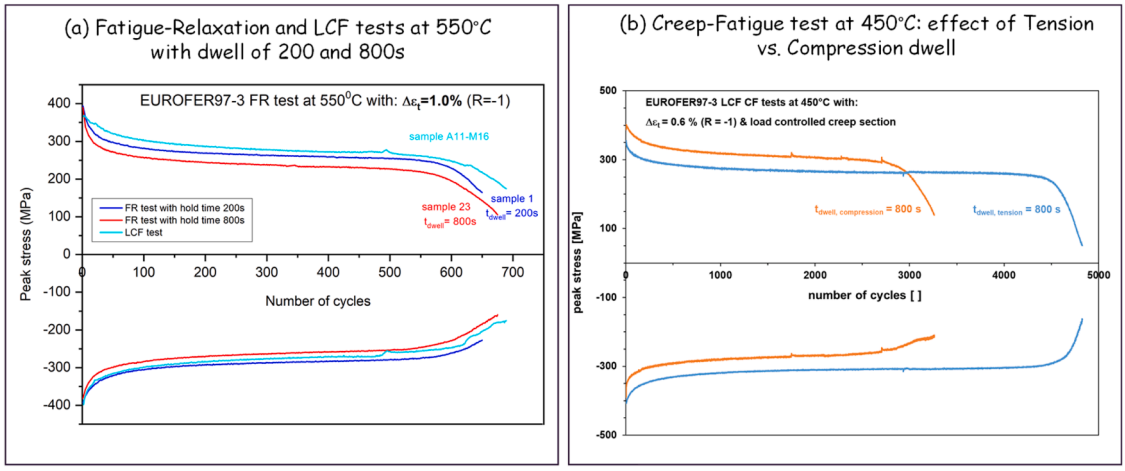


Fig. 16. (a, left) Example of Fatigue-relaxation test results: Fatigue-relaxation tests performed at 550 °C with dwell in tension compared to corresponding pure LCF test; and (b, right) creep-fatigue tests results revealing a weak effect of hold time and strong effect of the load sign at the dwell (i.e. compression vs. tension). Test conditions are specified on the legend.

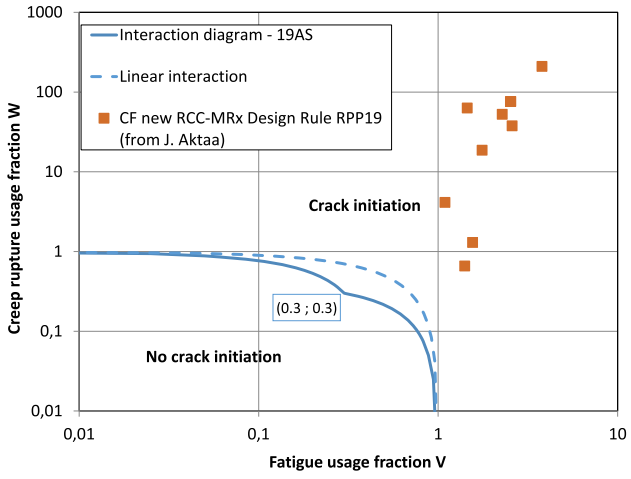


Fig. 17. Creep-fatigue interaction diagram built using RCC-MRx RPP19 creep-fatigue rule for cyclic softening steels and points coming from the C-F tests.

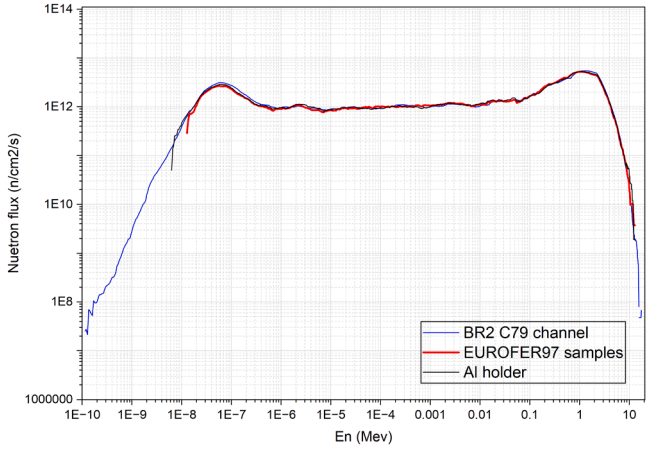


Fig. 18. Nuetron spectrum of BR2 C79 fuel channel. Spectrum is given for an empty fuel channel, for aluminum holder and Eurofer97 samples.

reference properties from the DEMO MPH, which are presented as average (solid) and minimum (dashed) curves. While the minimum

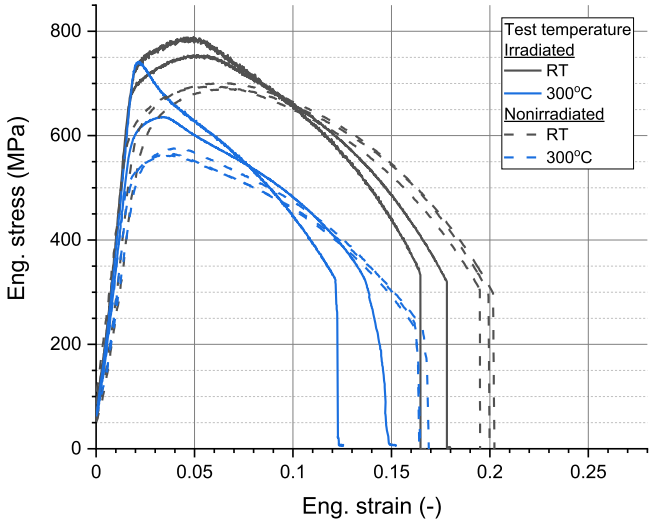
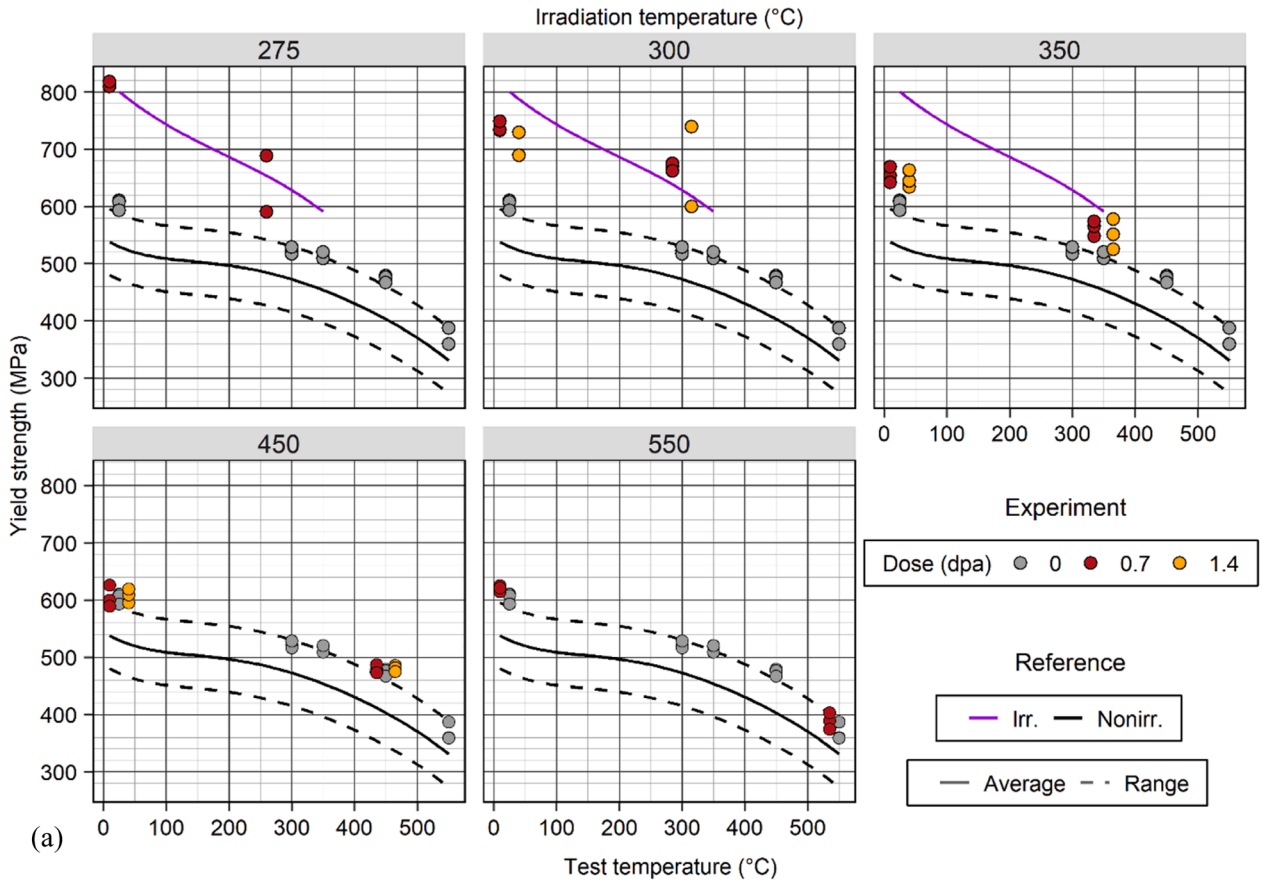


Fig. 19. Engineering stress-strain curves obtained for Batch 4 in reference and 1.4dpa_T_{irr}=300 °C condition.

curves are adopted directly from the MPH, where they were obtained by shifting the average curve downwards by 1.96·*SD* [13]. The strength of non-irradiated Batch 4 material is at the upper boundary of the reference range. Significant irradiation hardening observed after irradiation at 275 and 300 °C declines with the increase of irradiation temperature and vanishes above 350 °C.

Similarly, uniform elongation, as a measure of ductility, is shown in Fig. 20(c). The non-irradiated Batch 4 shows ductility below the average reference curve but within the range of uncertainty. Similarly to hardening, the irradiation-induced reduction of uniform elongation vanishes after irradiation above 350 °C. Fractography, not shown here but presented in Ref. [24], confirms high ductility of irradiated EUROFER in terms of area reduction and reveals the fracture mechanism by dimple rupture.

The main conclusion is the consistency of Batch 4 properties with formerly measured properties (from Batches 1 and 2) in the non-irradiated state. The observed irradiation induced damage effect at T_{irr}=275–300 °C is also consistent with the former findings. Finally, the irradiation at high temperature (450–550 °C), not earlier explored for EUROFER97, shows that at 450 and 550 °C the YS and UTS values are similar to the non-irradiated data points. This shows that high



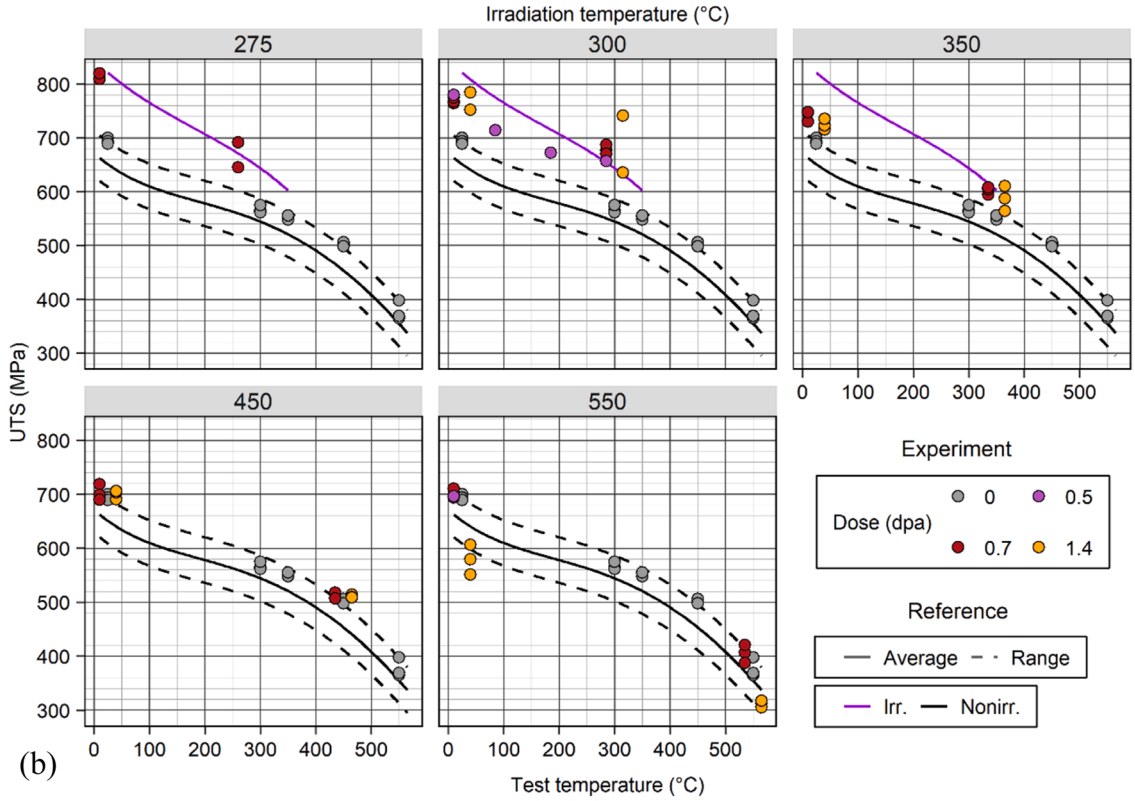


Fig. 20. Summary of tensile test results obtained for Batch 4 samples compared with EUROFER MPH average as well min-max curves. (a) yield stress; (b) UTS; (c) uniform elongation; (d) total elongation.

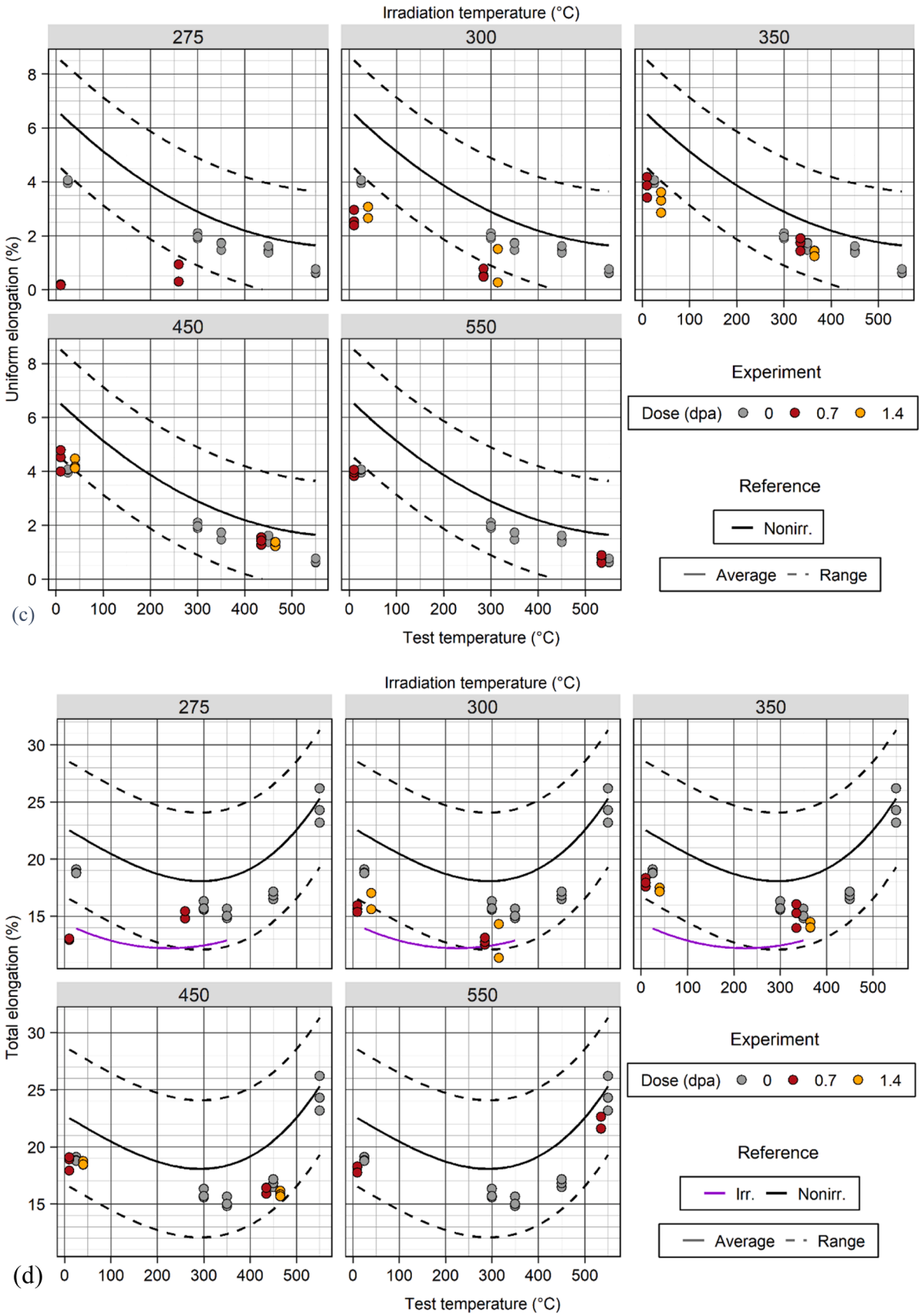


Fig. 20. (*continued*).

irradiation temperature does not cause hardening. However, further investigation and re-confirmation by both higher dpa level irradiation and validation by TEM microstructural analysis is required.

3.7. Plastic flow localization assessment

As reported in the section above, the low temperature irradiation causes early necking (i.e. zero uniform elongation) even at very low irradiation damage level as such as 1.4 dpa. This finding causes the need for the validation of the rule for the prevention of the immediate plastic flow instability under significant irradiation, which is given in the RCC-MRx code. The test matrix includes tensile tests on smooth and axisymmetric notched specimens at 20 and 300 °C, and four point bending tests on plain and notched specimens at 20 °C. Reference and neutron irradiated samples are to be tested. Only one irradiation condition is selected being ~2 dpa at irradiation temperature of 300 °C. Batch 3 was investigated. In total, 8 bending samples and 16 tensile samples were irradiated for this test campaign. The irradiation took place in the BR2 reactor, while the tests were performed inside of the hot cells. The tests are performed using both conventional displacement measurement (extensometer and crack mouth opening displacement (CMOD) clip gage) and stereo-digital image correlation techniques enabling 2 or 3D strain distribution acquisition. The latter is essential for the validation of the FEM model describing the plastic deformation, which in turn is needed to validate the IPFL prevention rule. The application of the digital acquisition of the lateral displacement also enables the direct calculation of the true stress during the plastic deformation even beyond the necking (at elongation higher than e_u). On Fig. 21(a) the reconstructed true stress – true strain curves at RT before and after the irradiation are shown. The true stress is calculated accounting for the Bridgman correction [32] (taking into account the radius of curvature at necking area), while the true strain is calculated based on the reduction of the cylindrical cross-section. The figure shows that in the non-irradiated sample the true stress nearly linearly increases after the UTS and reaches about 1 GPa at the rupture, corresponding to about 80% of true strain. These results are fully consistent with the calculation of the true stress and strain after fracture by post-mortem measurements. The neutron irradiation causes the increase of the yield stress, as expected, followed by a plateau at the level of UTS at ~1% true strain range, and then linear increase up to 1 GPa with the rupture at ~50% of true stress. These results confirm that even though engineering stress exhibits a pronounced drop (see example on Fig. 21) the true stress keeps on increasing showing the resistance of the material. The plateau observed at 1% true strain range likely originates from the superposition of the two processes: (i) softening caused by the absorption of dislocation loops by moving dislocations which clean the microstructure and form clear band channels [33–36] and (ii) hardening due to dislocation-dislocation interaction and pinning by grain boundary/lath interfaces and by precipitates [37]. The results for the four-point bending test of the sample with the V-shaped notch are presented on Fig. 21(b). In the case of non-irradiated test, one can see that the bending load leads to the resistance of the sample up to CMOD of 3 mm beyond which the force starts to decrease. In the non-irradiated sample, the force to initiate the bending is much larger, consistent with the irradiation hardening, but the inflection occurs nearly immediately as the threshold bending force is reached. This is apparently linked with ceasing of the uniform elongation. The detailed post-irradiation analysis and FEM modeling is ongoing with the objective of validation of the IPFL prevention design rule.

3.8. Irradiation creep

The irradiation creep was measured by using the conventional creep-pipe samples [38]. The geometry of the creep-pipes used in the study is shown in Fig. 22(a) together with the example of the photo of the sample before the irradiation (Fig. 22(b)) and location of the pipe diameter measurement points (Fig. 22(c)). The sample is filled with He at a given pressure that allows achieving the dedicated pressure at the irradiation temperature. Only one irradiation temperature was investigated being 300 °C. Six different pressure levels were applied to reach the equivalent hoop stress equal to 170, 192, 210, 230, 250 and 280 MPa. Batch 4 was investigated at 0.7 and 1.4 dpa (i.e. the same conditions for which the tensile data are reported). The creep deformation is calculated post-mortem after the irradiation by measuring the change of the pipe diameter. The measurements were done by SEM and optical profilometer with the precision of ~3–5 μm (actual precision depends on the surface finish of each specific test sample). Some images of the as-irradiated samples are provided on Fig. 22(d) and as one can see the edge of the pipes is well visible. The resulting creep deformation is provided on Fig. 23(a) and (b) for 0.7 and 1.4 dpa, respectively. For each irradiation condition at least two samples are inspected. The creep deformation is measured in three points on each pipe and the average value is reported together with the standard deviation. The green dashed curve shows the 0.5% deformation limit. One can see that given a statistical spread, all measured irradiation conditions do not impose the irradiation creep exceeding 0.5%. We also notice that the statistical spread is rather high, which is due to the accuracy of the measurement (linked with the absolute value of the creep pipe diameter). For that reason, we could not resolve any clear trend for the effect of the internal pressure on the creep deformation. As a recommendation, a larger diameter of the creep pipe is required to improve the accuracy in the creep deformation measurement if a higher resolution is required. Another alternative is to measure the irradiation induced stress relaxation [38].

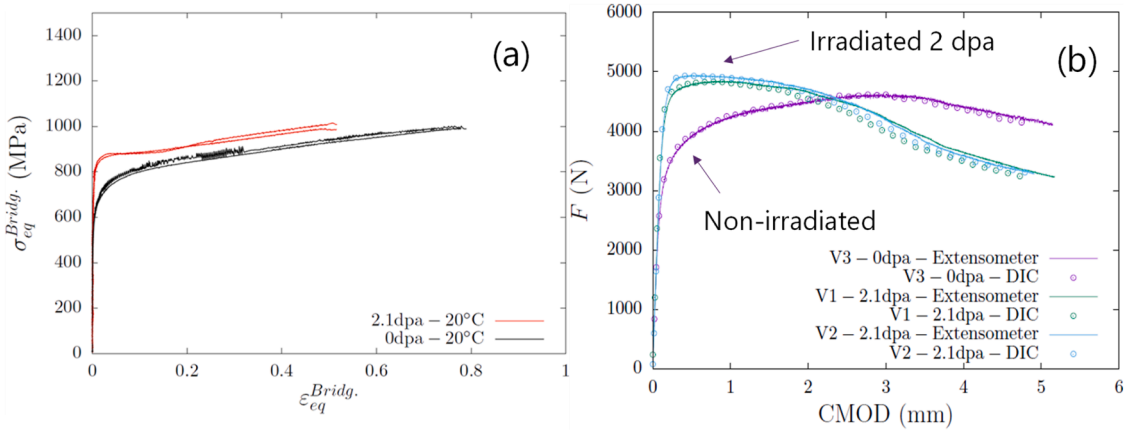


Fig. 21. Effect of neutron irradiation (2dpa_T_{irr}=300 °C) on (a) the true stress-true strain obtained using smooth round bar specimens; (b) force-CMOD of the four-point bend test performed on Batch 3.

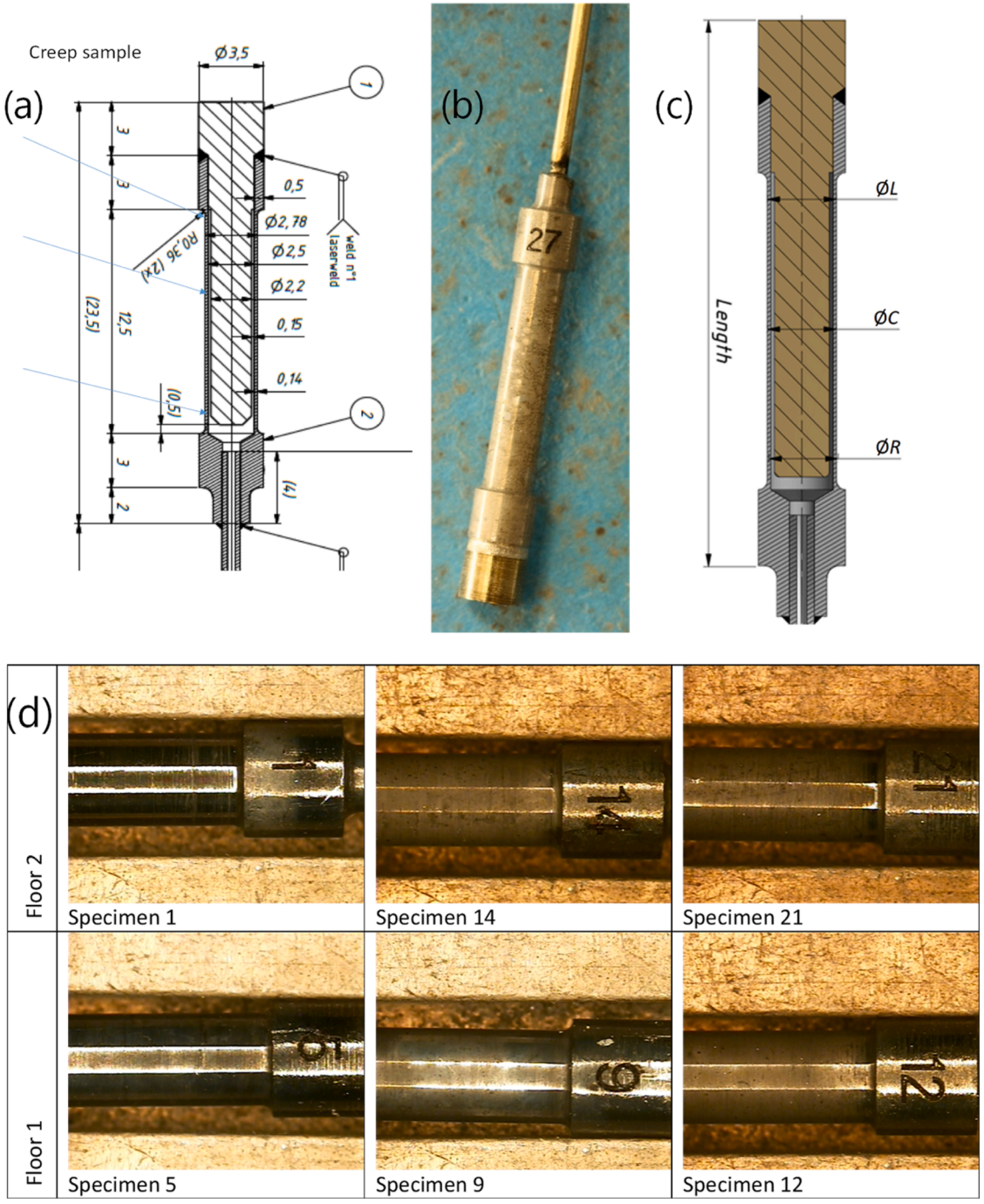


Fig. 22. Geometry of the creep pipes and photo images of the as-irradiated creep pipes used for the dimensional control after the irradiation.

3.9. *Effect of neutron irradiation on fracture toughness*

The evaluation of the effect of neutron irradiation on the fracture toughness is another large irradiation campaign that has been undertaken to provide the engineering mechanical properties for the design studies and design rules. The irradiation test matrix included the following conditions: 275/300, 350, 450 and 500 °C irradiation temperature and three irradiation damage levels 0.5, 1 and 2 dpa. The ductile fracture toughness is to be obtained according to ASTM E1820 standard at RT and irradiation temperature for each irradiation condition. Batch 3 was used for this investigation. The irradiation was performed on the reduced-size CT or DCT samples with the thickness of 8 mm. The sample geometry was taken according to the E1820 standard. The irradiation at 275 and 350 °C up to 2 dpa is still ongoing, while other test conditions are reached. At each irradiation condition (and non-irradiated state) at least three samples are tested. Given the issue spotted for the application of the UC techniques (see Section 3.3), it was decided to apply potential drop to perform the crack extension measurement during the test in addition to NDR and post-mortem examination. Fig. 24(a) shows the photo of the disk compact tension (DCT) facture toughness sample to which four wires are welded to enable the PD measurements. The clevises and pins applied to fix the sample at the test bench are located next to the sample. The results of the measurements after the irradiation at 275 °C_1dpa, in which the hardening and embrittlement is expected to be most severe given the tensile data, are presented in Fig. 24(b) and (c) for RT and T_{irr}. The results plotted are the

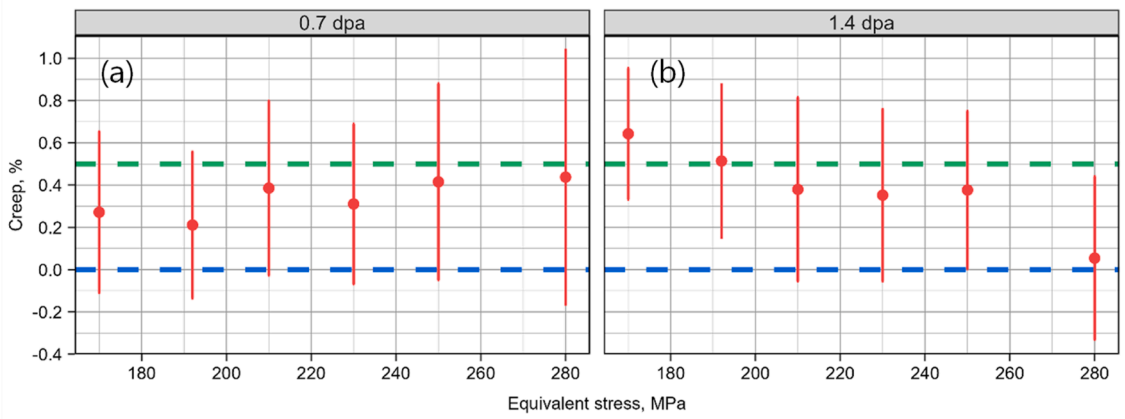


Fig. 23. Results of the creep measurements vs. hoop stress applied inside the creep pipes during the irradiation for (a) 0.7 dpa and (b) 1.4 dpa.

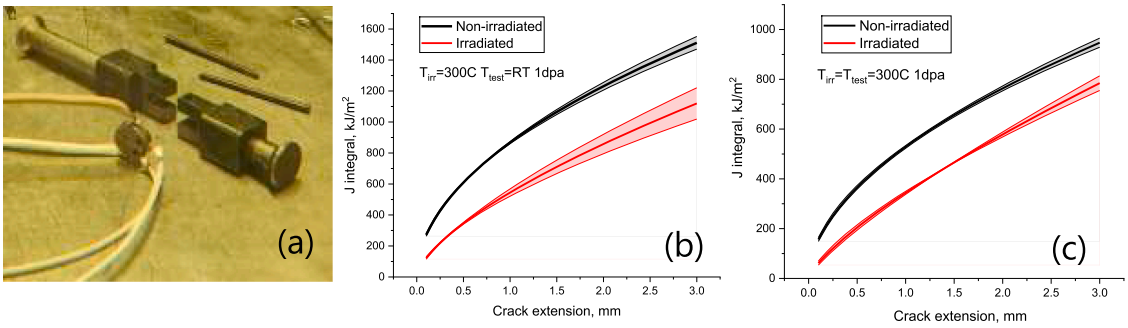


Fig. 24. (a) Setup for the fixation of the fracture toughness sample with welded wires for the PD techniques; (ii) J-r curves at T_{test}=RT for reference and 1dpa_300 °C irradiated Batch 3 samples; (ii) J-r curves at T_{test}=300 °C for reference and 1dpa_300 °C irradiated Batch 3 samples.

mean value of the resistance J-r curve obtained by averaging three curves, given that three samples per test condition were tested. The bars provide the standard deviation. One can clearly see that the irradiation hardening leads to the reduction of the J-r values. The reduction amount is comparable at the two test temperatures. The absolute values of the fracture toughness J_Q, obtained by NDR, are collected in Fig. 25 for all tests. One can appreciate that the statistical spread of the data is not significant, which reflects the homogeneity of the material and reproducibility of the test results in both reference and as-irradiated conditions. The J-r curves obtained at higher irradiation temperatures are provided in Fig. 25. The irradiation at 350 °C also causes the deterioration of the resistance against crack extension, as one can see on Fig. 25 (a), while at T_{irr}=450 and 500 °C the reduction of the J-r is just minor.

The J_Q values from all performed tests are summarized on Fig. 26. To guide the interpretation of the results arrows with digits 1, 2 and 3 are added on the figure. The digits signify the following observations:

(1) Reduction of J_Q for T_{irr}=275 °C and T_{irr}=350 °C at both test temperatures RT and Tirr;
(2) Reduction of J_Q for T_{irr}=450 °C and T_{irr}=500 °C only at RT test temperature;
(3) No measurable change of J_Q (given statistical spread) for T_{irr}=450 °C and T_{irr}=500 °C at T_{irr} test temperature.

These observations accordingly confirm the following:

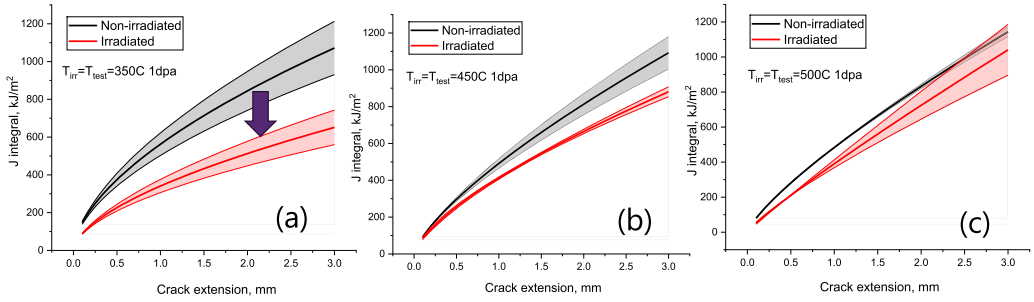


Fig. 25. J-r curves obtained at T_{irr}=T_{test} for reference and 1 dpa irradiated samples for (i) T_{irr}=350 °C; (ii) T_{irr}=450 °C and (iii) T_{irr}=500 °C.

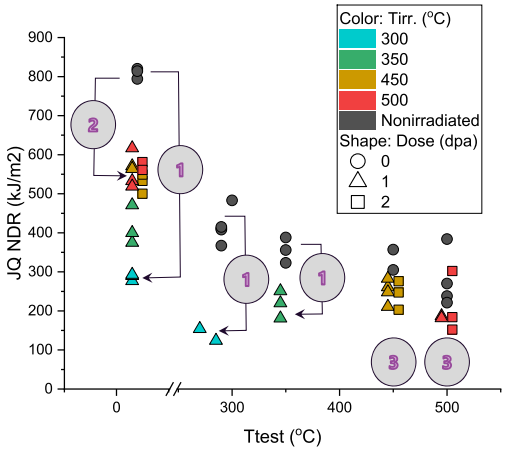


Fig. 26. J_Q vs. test temperature for reference and neutron irradiated samples. The irradiation conditions are shown on the legend.

low-temperature irradiation hardening revealed by tensile tests translated to the considerable reduction of the fracture toughness already at 1 dpa.

measurable deterioration of the crack resistance occurs at irradiation temperature of 350°C_1dpa, but less extended as compared to 275°C_1dpa, which is also consistent with the minor irradiation hardening and reduction of the total elongation registered at 350°C_0.7-1.4dpa.

at 450 and 550°C 0.7-1.4 dpa, tensile tests did not reveal the impact of the neutron irradiation. However, the fracture toughness at room temperature is measurably reduced at 450-500°C at 1 and 2 dpa damage dose. This demonstrates that at certain irradiation conditions the sole tensile property assessment is not sufficient to conclude on the fracture mechanics properties. As a hypothesis, the physical explanation for the observed "non-hardening embrittlement" (i.e. embrittlement taken as the reduction of the fracture toughness) may originate from the coarsening of the precipitates under high irradiation temperature or recovery of the initial microstructure (e.g. reduction of the dislocation density). These preliminary results obtained by the PD measurements or NDR analysis will have to be confirmed as far as possible using post-mortem observation of crack extension and by application of the basic procedure. In addition, the microstructural investigation using SEM-EBSD and TEM is required to validate the above proposed hypothesis. The latter is precluded due to the very high activation of the samples (> ten Sv/hour on contact on a single sample), therefore the fractured sample must be cut to extract small enough coupon for further focus ion beam TEM/SEM sample preparation.

4. Discussion

Based on the currently achieved results and issues faced during the implementation of the program, a number of lessons learned will be outlined below.

At first, we can notice that the microstructure of the Batch 3 plates is highly uniform and has limited variation from plate to plate as can be concluded from the various tests performed on different plates (different thickness) by different labs. Additionally, the characteristic sample volumes varied significantly i.e. from 20 mm thick fracture toughness samples down to 2 mm diameter tensile samples for the neutron irradiation. The interlaboratory LCF study has revealed rather limited data spread on the fatigue lifetime, which is typically obtained within a single lab test program. This is also an indirect confirmation of the good homogeneity of the tested material.

The fracture toughness campaign revealed an issue for the applicability of the UC technique to perform in-situ measurement of the crack extension. The UC signal underestimates or does not show the crack extension at all at the onset of the crack growth, which has been attributed to the non-planar crack growth, explaining high toughness and erroneous readings from the UC. The strongest deviation between J-r curve obtained by UC and NDR or Basic procedure was found for T_{test}= RT and 500 °C. In both cases, the J-r curve reconstructed based on the UC readings represents nearly a straight line parallel to the construction line. We explain this finding by the fact that at RT the crack was not kept in a single plane (that should be normal to the direction of the applied load) and various crack segments exhibited extensions in different planes, apparently signifying the high toughness of the material. As a result, the readings of UC for such crack configurations cannot provide an adequate description of the crack extension. At 500 °C, the maximal load is reached very early causing the necking deformation which apparently also provides certain corruption in the UC response precluding the correct crack extension measurement. The issue has been faced by all three labs assigned to perform this task, and it was registered for Batch 3 as well as Batch 4 products. For the non-irradiated samples, the multi-specimen approach and post-mortem crack extension measurements were applied. An in-depth discussion the fracture toughness test procedures and results for non-irradiated EUROFER97 Batch 3 and Batch 4 can be found in [39]. However, for the neutron irradiated specimens, whose number was initially defined based on the assumption that the UC would be applicable, the multi-specimen approach would require more samples to obtain the valid set according to ASTM or ISO norms. Given the situation, it has been decided to apply the potential drop technique and special procedure was developed to organize the welding of the PD wires to the fracture toughness samples inside the hot cell. The validation of the PD techniques was performed using T91 to save the material, and then was successfully applied to EUROFER97 neutron irradiated specimens. The recommendation to follow from this experience is to prioritize the test protocol for the fracture toughness testing of neutron irradiated specimens before the start of the irradiation campaign. The volume required for the irradiation of the fracture toughness specimens is by far larger than for tensile or bend bar specimens for the IPFL study. Therefore, the cost and irradiation time can be significantly affected by the decision on the number and geometry of the irradiated samples.

In general, qualification-acceptable irradiation volumes (for fracture toughness or LCF samples) are scarce in the available material test reactors. In the present study, the compromise and earlier available experience was applied to define the dimensions of the fracture toughness samples to generate meaningful results, still not necessary fully valid according to ASTM/ISO standards at high test temperature. With the currently available MTR facilities, the dimension of the samples imposed the limit on the maximum irradiation flux to be 0.5 dpa/year on BRR and 2 dpa/year on BR2 reactor. The application of high flux positions (flux trap), which is for instance a common practice at ORNL on HFIR or NRG on HFR would not offer sufficient cross-section to incorporate the fracture toughness samples. Adaptation of standards (or creation of a new standard) for SSTT for fracture toughness and LCF samples is required to enable usage of high flux MTR channels and exploitation of DONES.

The creep life of Batch 3 is found to be longer than that of Batch 1 and 2 at intermediate (400/450 °C) temperature. However, this finding became evident when the test program progressed by about two years, while the creep-fatigue and negligible creep tests were running in parallel. As a result, the initially assumed test parameters (based on the available Batch 1 and 2 experience) caused essentially longer test duration, delaying the implementation timeline and raising the budget. Preliminary quick screening high-temperature tensile, LCF and creep tests would enable the optimization of the test parameters for long C-F and creep tests.

The implementation of the bespoke tests for the validation of the efficiency diagram was achieved with a certain delay due to the supply of the equipment and instrumentation required for those tests. Given that limited labs are capable to perform such tests, the recommendation is to identify possible back-up laboratories (even if the work will have to be outsourced to the industry). The same applies to the high-temperature tests (above 550 °C) which in the present test campaign were performed in air, although the oxidation could have induced additional damage. However, the obtained properties are believed to be conservative and performing tests in vacuum should deliver even better performance. There is unfortunately a low availability of the vacuum furnaces instrumented for the long-term cyclic tests (with clip gages). The availability of such equipment inside of the hot cells is even unique. In case of the demand of the vacuum chamber for mechanical tests, a special call for the equipment validation is recommended to ensure the feasibility of implementation of such demand.

To summarize, below we provide a brief status of the current progress, for the scope listed in Table 2, subdivided into fully completed results, preliminary datasets and uncompleted high priority tests:

Fully completed programmes: uniaxial ratcheting; creep-fatigue tests; tensile data in non-irradiated state.
Preliminary datasets and data pending further validation: fracture toughness tests in non-irradiated and irradiated state; creep; tension-torsion cyclic ratcheting; fatigue crack growth; irradiation creep; immediate plastic flow localization in non-irradiated and irradiated state.
next step highest priority test campaigns: tensile properties at 2 dpa in the whole temperature range; test programme on TIG and HIP weldments.

5. Conclusions

The planned qualification test campaign for EUROFER97 has achieved a good progress during 2021–2025, although certain delays were incurred for various reasons as discussed above. The summary of the most important unexpected issues is provided in Section 4.

Based on the newly obtained LCF data, the updated temperature-range refined best-fit curves will be introduced in the RCC-MRx to account for the information obtained from the three EUROFER97 batches, as is required by the code. A good agreement for the fatigue life and cyclic softening behavior is obtained between Batch 1, 2 and Batch 3 results.

On the other hand, the creep life of Batch 3 is found to be significantly higher than that of Batch 2 at intermediate temperature. The difference originates from the larger yield stress and lower uniform elongation of the Batch 3. C-F tests were also successfully performed, and based on the outcomes of those tests the updated C-F design rule was not breached since no failure was observed in the safe region of the C-F interaction diagram.

The neutron irradiation campaigns were successfully launched to assess the modification of tensile, fracture toughness and irradiation creep properties. The results of the irradiation demonstrated expected aging at 275–350 °C expressed in the hardening and reduction of ductility. The reduction of the fracture toughness at RT-350 °C is found at such a low dose as 1 dpa. The irradiation creep deformation measured after the irradiation at 300 °C up to 1.4 dpa did not reveal significant irradiation creep. The high temperature irradiation at 450 and 550 °C did not reveal any measurable modification of the tensile properties, whereas the fracture toughness measured at RT after high temperature irradiation revealed the reduction. In addition, bespoke samples for the validation of the IPFL prevention rule have been irradiated and tested, clearly seeing the impact of the irradiation hardening. The post-processing of the obtained information is ongoing to validate the corresponding design rule in RCC-MRx. Part of the irradiation campaign (for 2 dpa) still needs to be completed in 2026.

The gaps related to the characterization of welds will need to be addressed after 2025, the following test campaigns for the tungsten inner gas (TIG) welds are currently planned:

(i) tensile properties at RT, 300 and 550 °C, cross-weld sample configuration
(ii) ductile fracture toughness at RT, 300 and 550 °C, notch along the weld line
(iii) low cycle fatigue at RT, 300 and 550 °C, cross-weld sample configuration
(iv) ductile fracture toughness and tensile properties should also be assessed after the neutron irradiation up to 0.5 and 1 dpa at 300, 350, 450 and 500 °C

The preparation of the Hot Isostatic Pressing (HIP) welds is just completed and its characterization will start asap.

CRediT authorship contribution statement

D. Terentyev: Writing – review & editing, Writing – original draft, Supervision, Software, Resources, Project administration, Methodology, Investigation, Funding acquisition, Data curation, Conceptualization. **P. Lamagnère:** Writing – review & editing, Writing – original draft, Methodology, Data curation. **Y. Lejeail:** Investigation. **G. Perez:** Investigation. **M. Walter:** Writing – review & editing, Investigation. **T.T. M. Nguyen:** Writing – review & editing. **M. Carrington:** Investigation. **C. Caes:** Writing – review & editing, Investigation. **E. Leon Gutierrez:** Investigation. **M. Serrano:** Writing – review & editing, Investigation. **N. García-Rodríguez:** Investigation. **R. Hernandez:** Investigation. **J. Hure:** Investigation. **J.B. Pontier:** Investigation. **E. Gaganidze:** Investigation. **J. Aktaa:** Investigation. **E. Perelli Cippo:** Investigation. **Dario Ripamonti:** Investigation. **V. Lezaud-Chaillioux:** Investigation. **A. Zinovev:** Writing – original draft, Investigation. **I. Szenthe:** Investigation. **D. Bernardi:** Investigation. **G. Pintsuk:** Resources, Project administration, Investigation, Funding acquisition. **G. Aiello:** Writing – review & editing, Funding acquisition. **Yann Carin:** Writing – review & editing. **Zmitko Milan:** Writing – review & editing. **Salvatore D'Amico:** Writing – review & editing. **Poitevin Yves:** Writing – review & editing.

Declaration of competing interest

The authors declare that they have no known competing financial interests or personal relationships that could have appeared to influence the work reported in this paper.

Acknowledgment

This work has been carried out within the framework of the EUROfusion Consortium, funded by the European Union via the Euratom Research and Training program (Grant Agreement No 101052200 — EUROfusion). Views and opinions expressed are however those of the author(s) only and do not necessarily reflect those of the European Union or the European Commission. Neither the European Union nor the European Commission can be held responsible for them.

Data availability

The data that has been used is confidential.

References

[1] G. Federici, Testing needs for the development and qualification of a breeding blanket for DEMO, Nucl. Fusion 63 (12) (2023) 125002.
[2] L.M. Giancarli, M.Y. Ahn, S. Cho, Y. Kawamura, A. Leal-Pereira, M. Merola, Y. Poitevin, I. Ricapito, Q. Sheng, H. Tanigawa, H. Tanigawa, J.G. van der Laan, X. Y. Wang, Status of the ITER TBM Program and overview of its technical objectives, Fusion Eng. Des. 203 (2024) 114424.

[3] R.-M. Afcen, Design and Construction Rules for Mechanical Components of Nuclear installations: High temperature, Research and Fusion Reactors, 2022 edition, 2022.
[4] M. Zmitko, N. Thomas, A. LiPuma, L. Forest, L. Cogneau, J. Rey, H. Neuberger, Y. Poitevin, The European ITER test blanket modules: progress in development of fabrication technologies towards standardization, Fusion Eng. Des. 109-111 (2016) 1687–1691.
[5] edited byL. El-Guebaly (Ed.), Status of European reduced Activation Ferritic/ Martensitic Steel EUROFER97 Published in the Book Fusion Energy Technology R&D Priorities, Elsevier, 2024. edited byISBN: 978–0–443–13629–0.
[6] F.E. Roadmap. https://euro-fusion.org/eurofusion/roadmap/, 2022.
[7] A. Kohyama, A. Hishinuma, D.S. Gelles, R.L. Klueh, W. Dietz, K. Ehrlich, Low-activation ferritic and martensitic steels for fusion application, J. Nucl. Mater. 233-237 (1996) 138–147.
[8] A.A.F. Tavassoli, E. Diegele, R. Lindau, N. Luzginova, H. Tanigawa, Current status and recent research achievements in ferritic/martensitic steels, J. Nucl. Mater. 455 (1–3) (2014) 269–276.
[9] G. Pintsuk, E. Diegele, S.L. Dudarev, M. Gorley, J. Henry, J. Reiser, M. Rieth, European materials development: results and perspective, Fusion Eng. Des. 146 (2019) 1300–1307.
[10] AFCEN, Guide for Introducing a New Material in the RCC-MRX, Technical Publication form AFCEN, 2017.
[11] F. Tavassoli, Eurofer steel, development to full code qualification, Procedia Eng. 55 (2013) 300–308.
[12] T. Lebarb, C. Pétesch, J. Muñoz-Garcia, Standardization of eurofer material, a first step toward industrialization, Fusion Eng. Des. 159 (2020).
[13] E. Gaganidze, F. Gillemot, I. Szenthe, M. Gorley, M. Rieth, E. Diegele, Development of EUROFER97 database and material property handbook, Fusion Eng. Des. 135 (2018) 9–14.
[14] E. Gaganidze, J. Aktaa, Assessment of neutron irradiation effects on RAFM steels, Fusion Eng. Des. 88 (3) (2013) 118–128.
[15] C. Cabet, E. Dalle, E. Gaganidze, J. Henry, H. Tanigawa, Ferritic-martensitic steels for fission and fusion applications, J. Nucl. Mater. 523 (2019) 510–537.
[16] J. Aktaa, M. Walter, G. Angella, E.P. Cippo, Creep-fatigue design rules for cyclic softening steels, Int. J. Fatigue 118 (2019) 98–103.
[17] G. Federici, W. Biel, M.R. Gilbert, R. Kemp, N. Taylor, R. Wenninger, European DEMO design strategy and consequences for materials, Nucl. Fusion 57 (9) (2017) 092002.
[18] F. Hernández González, BB HCPB design description document, EUROfusion report 2NXLFV (2021).
[19] Y. Dai, G.R. Odette, T. Yamamoto, The effects of helium in irradiated structural alloys, Compr. Nucl. Mater. 1 (2012) 141–193.
[20] A. Zinovev, P. Lamagnere, K. Poleshchuk, D. Terentyev, D. Bernardi, C. Cristalli, E. Leon-Gutierrez, N. García-Rodríguez, C. Caes, G. Pintsuk, G. Aiello, Low cycle fatigue of EUROFER97 investigated for test blanket modules of ITER: an interlaboratory study, J. Nucl. Mater. 597 (2024) 155127.
[21] K. Zhang, J. Aktaa, Ratcheting and fatigue behavior of Eurofer97 at high temperature, part 2: modeling, Fusion Eng. Des. 152 (2020) 111426.
[22] P. Matheron, G. Aiello, C. Caes, P. Lamagnere, A. Martin, M. Sauzay, Tension-torsion ratcheting tests on 9Cr steel at high temperature, Nucl. Eng. Des. 284 (2015) 207–214.
[23] C.C. Chang, D. Terentyev, A. Bakaev, A. Zinovev, D. Del Serra, P. Verleysen, T. Pardoen, Application of mini-flat and cylindrical test specimens to extract hardening law and ductility of neutron irradiated Eurofer97, Fusion Eng. Des. 216 (2025) 115072.
[24] A. Zinovev, C.C. Chang, J. Van Eyken, E. Gaganidze, D. Terentyev, Effect of neutron irradiation to 0.7 dpa and 1.4 dpa on the tensile properties and fracture surface of EUROFER97 steel, J. Nucl. Mater. 587 (2023) 154742.
[25] J.H. Lee, H.Y. Lee, S.G. Hong, S.B. Lee, Fatigue crack growth behavior of mod.9Cr-1Mo steel at elevated temperatures: effect of temperature, loading frequency and R ratio, J. Mech. Sci. Technol. 31 (8) (2017) 3665–3669.
[26] D. Pelowitz, J. Durkee, J. Elson, M. Fensin, M. James, R. Johns, G. McKinney, S. Mashnik, L. Waters, T. Wilcox, MCNPX 2.7. 0 Extensions, Los Alamos National Laboratory, 2011.
[27] A. Stankovskiy, G. Van den Eynde, L. Fiorito, ALEPH V.2.7, A Monte Carlo burn-up code, SCK•CEN, 2018.
[28] A. Plompen, Jeff-3.3, Nucl. Energy Agency (2017).
[29] D.A. Brown, M. Chadwick, R. Capote, A. Kahler, A. Trkov, M. Herman, A. Sonzogni, Y. Danon, A. Carlson, M. Dunn, ENDF/B-VIII. 0: the 8th major release of the nuclear reaction data library with CIELO-project cross sections, new standards and thermal scattering data, Nucl. Data Sheets 148 (2018) 1–142.
[30] A.Y. Konobeyev, U. Fischer, Y.A. Korovin, S. Simakov, Evaluation of effective threshold displacement energies and other data required for the calculation of advanced atomic displacement cross-sections, Nucl. Eng. Technol. 3 (3) (2017) 169–175.
[31] M. Norgett, M. Robinson, I. Torrens, A proposed method of calculating displacement dose rates, Nucl. Eng. Des 33 (1) (1975) 50–54.
[32] P.W. Bridgman, Journal of applied physics 18 (1947) 246–258.
[33] S.J. Zinkle, B.N. Singh, Microstructure of neutron-irradiated iron before and after tensile deformation, in: Symposium on Microstructural Processes in Irradiated Materials held at the Annual Meeting of the Minerals-Metals-and-Materials-Society, San Francisco, CA, 2005, pp. 269–284.
[34] D. Terentyev, D.J. Bacon, Y.N. Osetsky, Reactions between a 1/2 < 111 >screw dislocation and < 100 >interstitial dislocation loops in alpha-iron modelled at atomic scale, Philos. Mag. 90 (7–8) (2010) 1019–1033.
[35] D. Terentyev, P. Grammatikopoulos, D. Bacon, Y. Osetsky, Simulation of the interaction between an edge dislocation and a <100>interstitial dislocation loop in α-iron, Acta Mater. 56 (2008) 5034–5046.
[36] D. Terentyev, Y.N. Osetsky, D.J. Bacon, Competing processes in reactions between an edge dislocation and dislocation loops in a body-centred cubic metal, Scr. Mater. 62 (9) (2010) 697–700.
[37] D. Hull, D.J. Bacon, Introduction to Dislocations, Butterworth-Heinemann, Oxford, 2001.
[38] N.V. Luzginova, M. Jong, J.W. Rensman, J.B.J. Hegeman, J.G. van der Laan, Irradiation-induced stress relaxation of Eurofer97 steel, J. Nucl. Mater. 417 (1–3) (2011) 104–107.
[39] E. Gaganidze, D. Terentyev, M. Serrano, P. Lamagnère, M. Walter, T.T.M. Nguyen, A. Zinovev, D. Bermúdez-Parra, G. Pintsuk6, G. Aiello, M. Zmitko, Y. Poitevin, Fracture toughness of European reference RAFM steel EUROFER97, J. Nucl. Mater. Rev. (2026).